ARA

STRUCTURAL MEASURES OF DUCTILITY

FOR

TITANIUM ALLOY Ti-6Al-4V AND 18% NICKEL MARAGING STEEL (250)

Ralph Papirno
Peter Kyle

Final Technical Report No. ARA-336-4

1 August 1967

Prepared For

Contract No. NASw-1423

National Aeronautics and
Space Administration
Washington, D. C.

ALLIED RESEARCH ASSOCIATES, INC.
VIRGINIA ROAD · CONCORD, MASSACHUSETTS

Structural Measures of Ductility

for

Titanium Alloy Ti-6Al-4V
18% Nickel Maraging Steel (250)

SUMMARY

The effect of ductility in a structure containing stress concentrations is to lessen the severity of the geometric discontinuities associated with the stress concentrations by local yielding, which in turn results in a continuous decrease in stress concentration factor until fracture occurs. One measure of this structural ductility effect is a parameter called the ductility ratio, $\bar{e}$, which may be obtained from strength tests of notched tension specimens. In ductile materials $\bar{e} = 0$, in brittle materials $\bar{e} = 1$ and in limited ductility materials $0.02 < \bar{e} < 1$. In this investigation notch tests on aged titanium alloy, Ti-6Al-4V and aged 18% nickel maraging steel were performed using specimens with a range of elastic stress concentration factors from 3 to 13.5 to evaluate the ductility ratio. The test results followed the relation $k_p = 1 + (k_e - k_{eo})\,\bar{e}$ where k_p and k_e are plastic and elastic concentration factors, k_{eo} is the elastic concentration factor below which the material is notch insensitive and $\bar{e}$ is the ductility ratio. The steel material displayed marked anisotropy in ductility behavior exhibiting notch insensitivity in the longitudinal direction and notch sensitivity in the transverse direction.

Average four-mil gage length permanent strains, measured along the fracture using photogrid techniques, were approximately 60% - 65% with some observations of strains higher than 100% for both materials. The two-inch gage length strain values averaged approximately 7% for the titanium and 2.5% for the steel material.

Metallographic examination revealed large and small grain size areas in the steel. Evidence is presented to show a possible connection between scatter of data for high k_e notch tests and the nonhomogeneous granular constitution of the steel material.

Ductility ratio and strength data for steel in the transverse directions are in good agreement with Gerard's strength-ductility relation for limited ductility materials, $\sigma_{tu}/\rho = 1.6 \times 10^6\,\bar{e}^{-1/6}$, while the titanium data are not. The lack of agreement of the titanium data is believed to be associated with their low values of ductility ratio, placing these materials outside of the limited ductility category. Design data for all the materials are presented and the efficiency of the materials in design is compared.

TABLE OF CONTENTS

LIST OF FIGURES

LIST OF FIGURES (Continued)

LIST OF FIGURES (Continued)

LIST OF TABLES

LIST OF SYMBOLS

A	Constant
a_1, a_2	Ligament width in notched specimens, in. (mm)
C_1, C_2	Constants
D	Hole diameter, in. (mm)
d	Notched specimen total ligament width, $d = a_1 + a_2$, in. (mm)
E	Modulus of elasticity, psi (N/mm^2)
E_{sm}	Secant modulus of maximum stress at stress concentration, psi, (N/mm^2)
E_{sn}	Secant modulus of net section stress, psi (N/mm^2)
e	Ductility parameter, $e = E_{sm}/E_{sn}$
$\overline{e}$	Ductility ratio
k_e	Elastic stress concentration factor
k_{eo}	Limiting value of k_e for notch insensitivity
k_p	Plastic stress concentration factor
L	Internal slot half-length, in. (mm)
r	Notch-end radius, in. (mm)
S	Structural strength, psi (N/mm^2)
t	Sheet thickness, in. (mm)
w	Specimen width, in. (mm)
ϵ_b	Brittle strain
ϵ_f	Failure strain
ϵ_o	Zero gage length strain
ϵ_2	Two-inch gage length strain
ϵ_4	Four-mil gage length strain
ρ	Density, $lb/in.^3$ (kg/mm^3)
σ_{tu}	Ultimate tensile strength, psi (N/mm^2)

STRUCTURAL MEASURES OF DUCTILITY

FOR

TITANIUM ALLOY Ti-6Al-4V AND 18% NICKEL MARAGING STEEL (250)

1. Introduction

Static tension failures in structural elements generally originate at stress concentrations resulting from geometric discontinuities. These discontinuities are inherent in the design, in which case the value of the associated elastic stress concentration factor can be determined; or the discontinuities can arise from fabrication processes and the values of the resulting elastic concentration factors, although of high value, are not determinate. Efficient structural design using a failure criterion should be based upon actual structural strength. This is related to the ultimate tensile strength of the material modified by the value of the stress concentration factor in the structure which is operative at failure and which is not necessarily the elastic value. Stress concentration factors in a structure remain at a constant value under increasing stress providing that the maximum stress in the concentration remains elastic . As the maximum stress in the concentration increases into the plastic region, local yielding relieves the severity of the geometric discontinuity and the stress concentration factor decreases. This decrease continues with increasing stress until fracture occurs. The degree to which the stress concentration factor is reduced from its elastic value to the value at fracture by plastic yielding is related to a measureable ductility property of the material of construction which we have called structural ductility.

The objective of the investigation described herein has been to study structural ductility both theoretically and by means of experiments on two high strength materials: titanium alloy Ti-6Al-4V and 18% nickel maraging steel (250). These studies have been restricted to the case of the response of materials to elastic stress concentration factors in the range of 3 to 13.5. This range of values includes those which ordinarily would be found in structural design and those which would result from mild radius nicks and flaws. The stress concentration factors associated with cracks and sharp flaws are of high numerical value and predictions of the fracture stress involve predictions of the stress required to propagate a sharp crack. The methods of crack propagation prediction have been developed using the analytical techniques of fracture mechanics and are not part of the current study.

The investigation included extensive testing to obtain notch strength, stress-strain and ductility properties, and also the development of a semi-empirical analytical relation between elastic and plastic stress concentration factor.

2. Elastic and Plastic Stress Concentrations

Materials have been classified into one of three ductility categories on the basis of the two-inch gage length fracture strains as: adequate ductility (roughly $\epsilon_2 > 10\% - 15\%$), limited ductility (roughly $10\% > \epsilon_2 > 1\%$) and brittle (roughly $\epsilon_2 < 1\%$). Materials can be classified into these same ductility categories on the basis of their fracture strength in the presence of stress concentrations. Using this structural behavior criterion, adequate ductility materials are those in which local yielding reduces the severity of geometric discontinuities to such an extent that the operative stress concentration at failure is essentially unity. For these materials the structural strength (S) and the material strength (σ_{tu}) are the same, i.e. $S = \sigma_{tu}$. In limited ductility materials local yielding is limited and serves to reduce stress concentration factors somewhat from the elastic value to a lower plastic value (k_p). Here the structural strength factor is reduced by the plastic concentration factor or $S = \sigma_{tu}/k_p$. Little relief of stress concentrations is possible with brittle materials. The structural strength is reduced from the material strength by the elastic stress concentration factor and may be given approximately by $S = \sigma_{tu}/k_e$. Materials which have been classified in the adequate ductility category on the basis of their two-inch gage length fracture strains will generally fall into the same category using a structural behavior criterion. However, the two-inch gage length strain is generally unreliable for classification of structural behavior for limited ductility materials and has limited value for the brittle category; in most cases the two-inch gage length strain classification is conservative with respect to structural ductility behavior. There is great interest in those materials which are in the structurally classified limited ductility category because these materials generally have the highest strength-to-weight ratios and have many potential applications. Test programs are required to obtain the appropriate design information. Standard information such as the two-inch gage length fracture strain is not directly applicable to structural design. Other structural ductility measures are required which are based upon the relations between structural strength, tensile strength and stress concentration factor.

Plastic Stress Concentrations

Structural strengths for adequate ductility and brittle materials are derived from relatively easily obtained parameters such as the ultimate tensile strength for the former and ultimate tensile strength and elastic concentration factor for the latter. The basic problem with such materials is one of identifying that the particular material is truly in the adequate ductility or brittle category. For the limited ductility class of materials strength predictions are based upon the plastic stress concentration factor at fracture which is related to both the elastic concentration factor and the ductility characteristics.

Previously Hardrath and Ohman (1) had shown that the plastic stress concentration factor obtained from notched bars may be expressed as

$$k_p = 1 + (k_e - 1)(E_{sm}/E_{sn}) \tag{1}$$

where

k_p = ultimate tensile strength/notched tensile strength

E_{sm} = secant modulus of the maximum stress at the stress concentration

E_{sn} = secant modulus of the net section stress in the structure.

There have been a number of variations of Eq. (1) based upon specific assumptions on the structure tested. The ratio of the secant moduli obtained may be designated as a structural ductility parameter as was suggested in Ref. 2. Eq. (1) can be written in the form

$$k_p = 1 + (k_e - 1)e \tag{2}$$

where

$e = (E_{sm}/E_{sn})$.

In limited ductility materials with higher elastic stress concentration factors, fracture occurs when the net section stress is elastic. Under these conditions, $E_{sn} = E$ and the ductility parameter is a constant for a given material. Designating the constant ductility parameter as $\bar{e}$, called the <u>ductility ratio</u>, it was shown in Ref. 2 that this parameter was the ratio of two strain values

$$\bar{e} = \epsilon_b/\epsilon_f \tag{3}$$

where ϵ_b is the brittle component of strain, given by $\epsilon_b = \sigma_{tu}/E$ and ϵ_f is the small gage length fracture strain at the stress concentration defined by $E_{sm} = \sigma_{tu}/\epsilon_f$.

Returning to Eq. (2), the implication is that for all values of k_e greater than unity, k_p will always be greater than unity. However from intuitive reasoning one could imagine a material on the borderline between limited ductility and adequate ductility materials which has sufficient ductility to relieve the effects of low value stress concentrations but which is notch sensitive to higher values of stress concentration factor. Such a material would have a threshold value of stress concentration factor above which it is sensitive and which can be designated as k_{eo}. The behavior of this material can be characterized by two relations

$$k_p = 1 \qquad \text{for } k_e \leq k_{eo} \tag{4}$$

and approximately by

$$k_p = 1 + (k_e - k_{eo})\bar{e} \qquad \text{for } k_e > k_{eo} \tag{5}$$

This behavior is illustrated schematically in Fig. 1. This representation is approximate because in a real material we would not expect to find discontinuities such as is represented by the point $k_p = 1$, $k_e = k_{eo}$.

It is important to note that implied in the representation shown in Fig. 1 is a constant value of the ductility ratio. As such, the ductility ratio may be considered a basic structural ductility property of materials. The threshold value of elastic stress concentration, k_{eo}, is also related to structural ductility behavior, however its value may also be influenced by the geometric size and configuration of the stress concentration. The full significance of this factor as a structural ductility parameter is not altogether clear at this time.

In the experiments which are described in the following sections of this report, structural ductility data were obtained for comparison with Eqs. (4) and (5) using the results of notch tests.

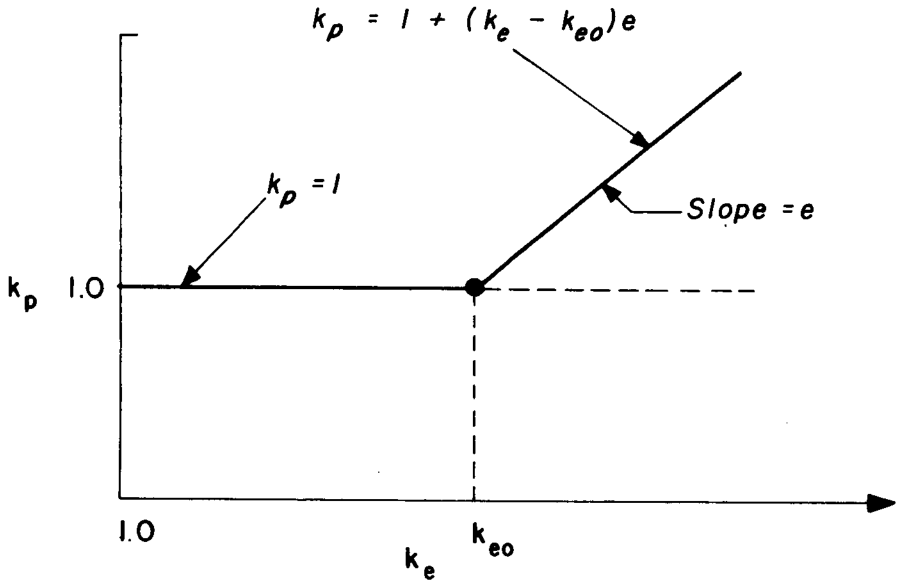

Figure 1. Elastic and Plastic Stress Concentrations for Limited Ductility Materials, Schematic.

6201

3. Experimental Procedures

The basic experiments in the program were a series of tensile tests on aged titanium alloy Ti-6Al-4V and aircraft quality, cold rolled aged 18% nickel maraging steel (250) in sheet form. Appropriately shaped specimens were machined for obtaining a) stress-strain properties and ultimate tensile strength, b) notch strength, c) small gage length strain and d) two-inch gage length permenent strain. Dogbone shape flat specimens of various proportions were used for all but the notch specimens. For the latter an internally notched configuration was designed to have the maximum elastic stress concentration factor for the given geometry. The details of the notch specimen design are given below.

Internal Notch Design

The basic advantage of an internally notched sheet tensile specimen is that the bending stresses which may develop in the specimen as a result of eccentricities in the loading train appear at the specimen sides while in the conventional externally notched specimens such bending stress would appear at the stress concentration at the root of the notch. This advantage more than offsets the greater manufacturing difficulties for the internally notched over the externally notched specimens.

The notch configuration we chose to employ was one we had used previously (2, 3) and is shown in Fig. 2. Dixon (4) derived relations for determining the stress concentration factor for such notches and these were extended and tested photoelastically by Papirno (5). For such a notch the theoretical elastic stress concentration factor is given by

$$k_e = \left[\frac{d/w}{2 - d/w}\right]^{1/2} \left[1 + 2(L/r)^{1/2}\right] \tag{6}$$

In our previous investigations we obtained a series of desired elastic stress concentration factors by varying the slot-end hole radius, while holding the other dimensions constant. The value of d/w previously employed was more or less arbitrarily chosen. However, an examination of Eq. (6) indicated that a maximum k_e value would exist as a function of d/w. This is of interest in notch specimen design since it is desirable to employ the geometry yielding the maximum k_e for a given notch-end radius. The notches are machined by drilling two holes and cutting a slot between them; the hole radius is then the notch end radius. There is a lower limit to hole radius that can be achieved with mechanical drills yielding cylindrical holes and at this lower limit it is desirable to use geometry which results in maximum k_e.

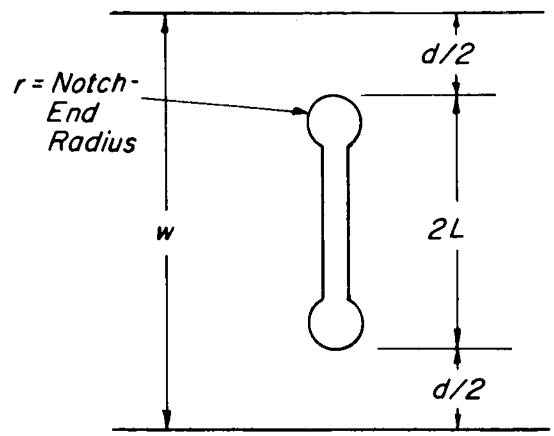

Figure 2. Internal Notch Configuration

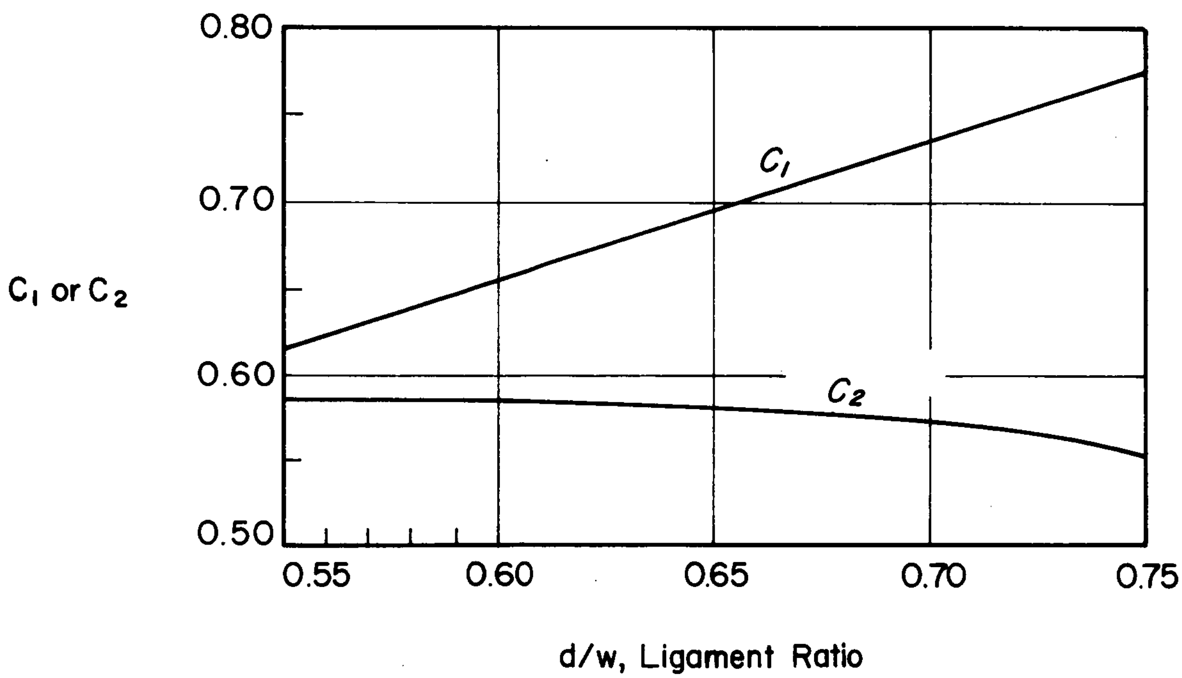

Figure 3. Values of the Constants C_1 and C_2 in the Elastic Stress Concentration Relation $k_e = C_1 + C_2(w/r)^{1/2}$

A maximization procedure used on Eq. (6) indicated that k_e would be a maximum for $d/w = 0.6$. Substituting this value in Eq. (6) results in

$$k_{e_{max}} = 0.654 \left[1 + 2 (L/r)^{1/2} \right] \tag{7}$$

Eq. (7) was used as a design relation for the notch specimens tested in the program. Because of manufacturing tolerances it is not always possible to achieve the optimum value of d/w in each specimen manufactured. This is especially true for the specimens with the smaller hole-sizes. After the specimens are manufactured and measured, specimen values of k_e can be determined by substitution of the appropriate measured dimensions into Eq. (6).

Computations of k_e based upon Eq. (6) can be considerably simplified by eliminating the factor L from the equation. This results in an expression of the form

$$k_e = \left[\frac{d/w}{2 - d/w} \right]^{1/2} + \left[\frac{d/w}{2 - d/w} \right]^{1/2} \left[2 - 2d/w \right]^{1/2} \left[w/r \right]^{1/2} \tag{8}$$

It is possible to express Eq. (8) in simplified form as

$$k_e = C_1 + C_2 (w/r)^{1/2} \tag{9}$$

where

$$C_1 = \left[\frac{d/w}{2 - d/w} \right]^{1/2}$$

$$C_2 = \left[\frac{d/w}{2 - d/w} \right]^{1/2} \left[2 - 2d/w \right]^{1/2}$$

Values of C_1 and C_2 for a range of d/w are given in Fig. 3.

Specimen Materials

The two test materials were in sheet form and all specimens were manufactured from a single sheet of each material. The major direction of rolling, as indicated by the manufacturer was designated as the longitudinal direction. The as-received sheet dimensions and other manufacturer supplied data are given in Tables 1 and 2.

Table 1: Manufacturer's Data for Titanium Alloy Ti-6Al-4V

1.	Identification	TMCA Heat G2038, Annealed
2.	Sheet Size	0.045 in thick x 36 in x 96 in. (1.14 mm x 890 mm x 2940 mm)[1]
3.	Composition, Percent	see below
4.	Annealed Mech'l Properties	see below

Composition, Percent:

Al	V	C	Fe	N	H	O	Ti
6.0	4.0	0.023	0.05	0.009	0.007	0.11	Rmdr.

Annealed Mech'l Properties:

	Yield Strength psi	Yield Strength (N/mm^2)	Ultimate Strength psi	Ultimate Strength (N/mm^2)	Elong. Percent
Long.	137,900	(950)	146,200	(1007)	13.0
Trans.	133,600	(920)	141,300	(975)	13.0

Table 2: Manufacturer's Data for Aircraft Quality 18% Nickel Maraging Steel (250)

1.	Identification	U.S. Steel Heat 1-0347, Cold Rolled, Annealed
2.	Sheet Size	0.040 in. thick x 29.6 x 120 in. (1.01 mm x 752 mm x 330 mm)
3.	Composition, Percent	see below
4.	Annealed Mech. Properties	not given

Composition, Percent:

C	Mn	P	S	Si	Ni	Cr	Mo	Ti	Cu	Fe
0.03	0.04	0.004	0.006	0.08	17.96	8.08	4.8	0.42	0.17	Rmdr.

The sheets were marked into sections to establish a sampling pattern and specimen blanks were cut. The titanium alloy blanks were first solution heat heated and the specimens were fabricated from the solution treated blanks. The steel specimens were fabricated from the annealed material. Both materials were aged after the specimens had been manufactured. The heat treating procedures were as follows:

Titanium Alloy Ti-6Al-4V:

Solution Treat: 1675F(1185K), Vacuum, 30 min.; W.Q. within 2-3 secs.

Aging: 900F(755K), Vacuum, 16 hrs.; FC

1 Throughout this report dimensions are given in the English system followed in parenthesis by the metric equivalent in the SI System. Metric length units in the text and in all drawings are in millimeters unless otherwise noted.

18% Maraging Steel (250):

Aging: 900F(755K), 3 hrs.; AC

Hardness values were taken after the aging heat treating. For the titanium alloy the values ranged from R_c35 to R_c38 while for the steel the range of values was from R_c50 to R_c52.

Specimen Preparation

a) Sampling Pattern: The sheets were marked in lettered panel sections as shown in Fig. 4 and groups of longitudinal and transverse specimen blanks were sheared oversize from each of the panels keeping well away from the original edges of the sheet. A typical sampling pattern from Section B is shown in Fig. 5. The other sections had similar sampling patterns. The specimen blanks were numbered to indicate the location in the sheet from which they were taken and the direction; for example in the specimen number designation SBT-13, the initial "S" designates steel, the "B" is for Section B of the sheet, the "T" indicates a transverse specimen and the final number designates this specimen as the 13th taken from the section. All specimens but those employed to obtain the two-inch gage length elongation were manufactured from blanks which were approximately 1.12 in. x 6 in. (28.4 mm x 152 mm). For the latter, the blanks were the same width but approximately 9.0 in. (228 mm) long.

b) Internally Notched Tensile Specimens: Specimens of the dimensions shown in Fig. 6 were manufactured with a range of slot-end hole sizes to obtain a range of elastic stress concentration factors from 3-13.5. The loading holes and outer contours of the specimen were machined first using standard machine shop practice. Rivet holes were drilled at the specimen ends using a drill jig, for later installation of end reinforcing plates. The central slot was introduced by first drilling and reaming the notch-end holes and then by cutting a slot between the holes using a 0.006 in. (0.15 mm) thick piercing saw. The saw blade was introduced through a 0.03 in. (0.75 mm) central hole in the specimen and separate cuts were made to the notch-end holes. The surfaces of the latter were protected by appropriate diameter wires placed in the holes prior to sawing.

Hole diameters to obtain the desired range of elastic stress concentration factors were determined from the relation given below, which results from rearranging terms in Eq. (7):

$$D = 2w \left[\frac{0.586}{k_e - 0.654}\right]^2 \qquad (10)$$

6306

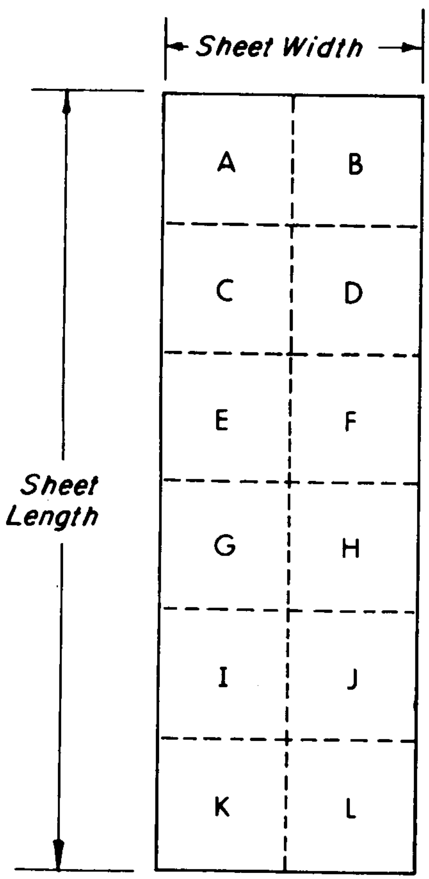

Figure 4. Sampling Panel Layout of As-received Sheet

6349

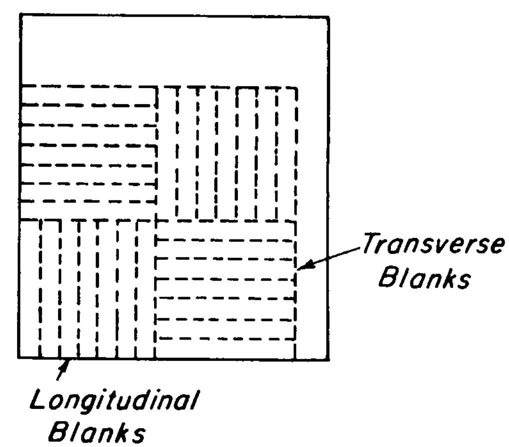

Figure 5. Sampling Pattern of Longitudinal and Transverse Specimens in one Sampling Panel

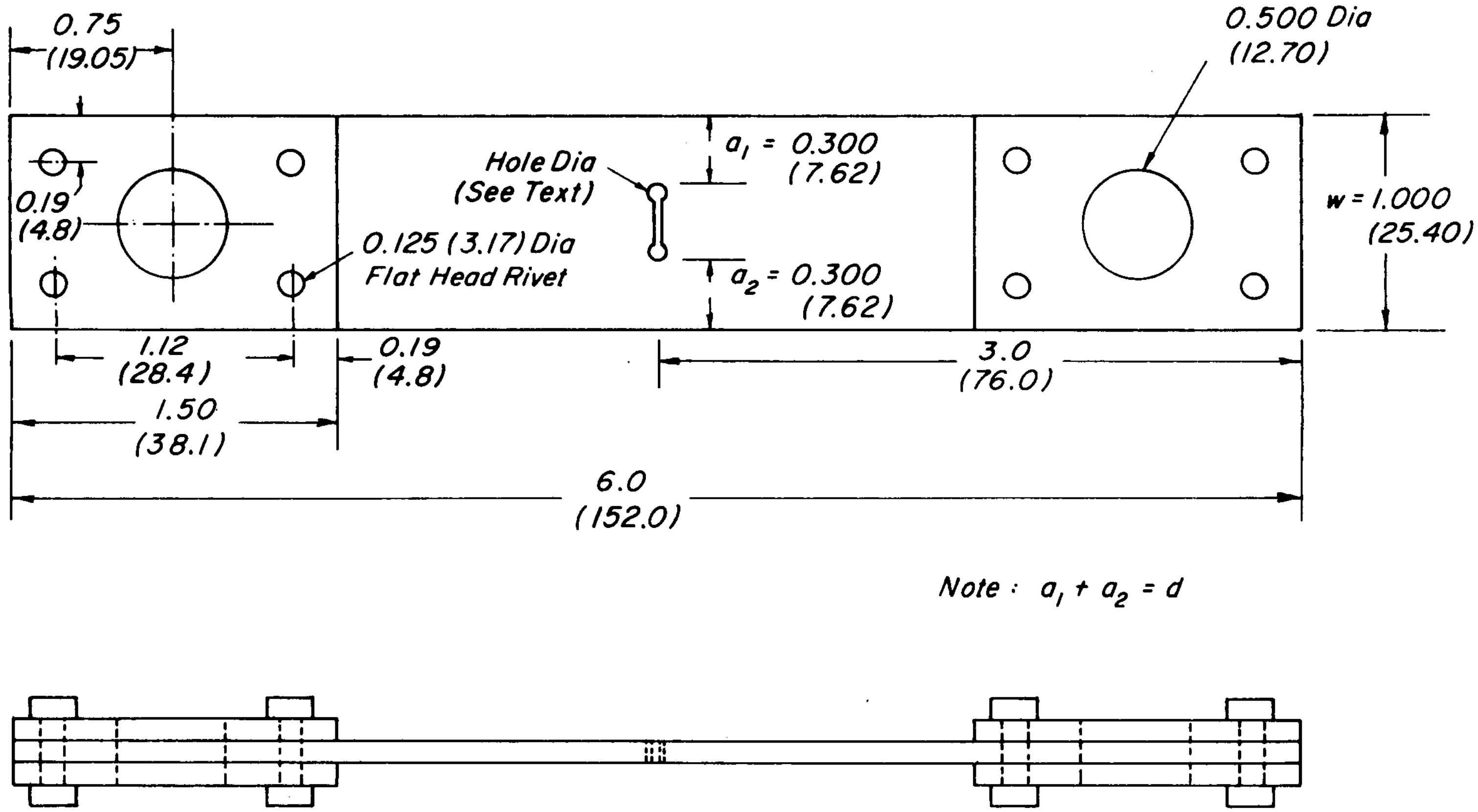

Figure 6. Notch Specimen Dimensions

Notched-end hole sizes were taken as those of the reamer size. The various drill and reamer sizes used for specimen manufacture are given in Table 3. It should be noted that drilling and reaming accurately located holes whose finished diameter is less than 0.012 in. (0.30 mm) where the material thickness may be as high as 10-12 times the hole diameter, is far from a routine operation. We employed a Derbyshire micro-drill press equipped with a compound rest as shown in Fig. 7. The technician constantly observed the specimen surface with the binocular microscope shown in the figure throughout the entire drilling and reaming operation.

Table 3. Drill and Reamer Sizes for Notch-End Holes

Elastic Conc.	Reamer Diameter		Drill Diameter	
Factor, k_e	in	mm	in	mm
3	0.1250	3.18	0.1200	3.05
4	0.0625	1.587	0.0595	1.51
5	0.0360	0.914	0.0330	0.838
6	0.0240	0.609	0.0210	0.533
7	0.0173	0.434	0.0150	0.381
8	0.0128	0.325	0.0116	0.294
9	0.0098	0.249	0.0089	0.226
10	0.0079	0.201	0.0071	0.180
11	0.0066	0.167	0.0060	0.152
12	0.0055	0.140	0.0050	0.127
13	0.0046	0.117	0.0042	0.107
13.5	None*		0.0042	0.107

* In this case only a drill was used and the concentration factor was computed from the drill diameter.

c) Sheet Tensile Specimens: Specimens with various gage lengths were employed for stress-strain properties, ultimate tensile strength, two-inch gage length permanent deformation, and small gage length strain. The dimensions of

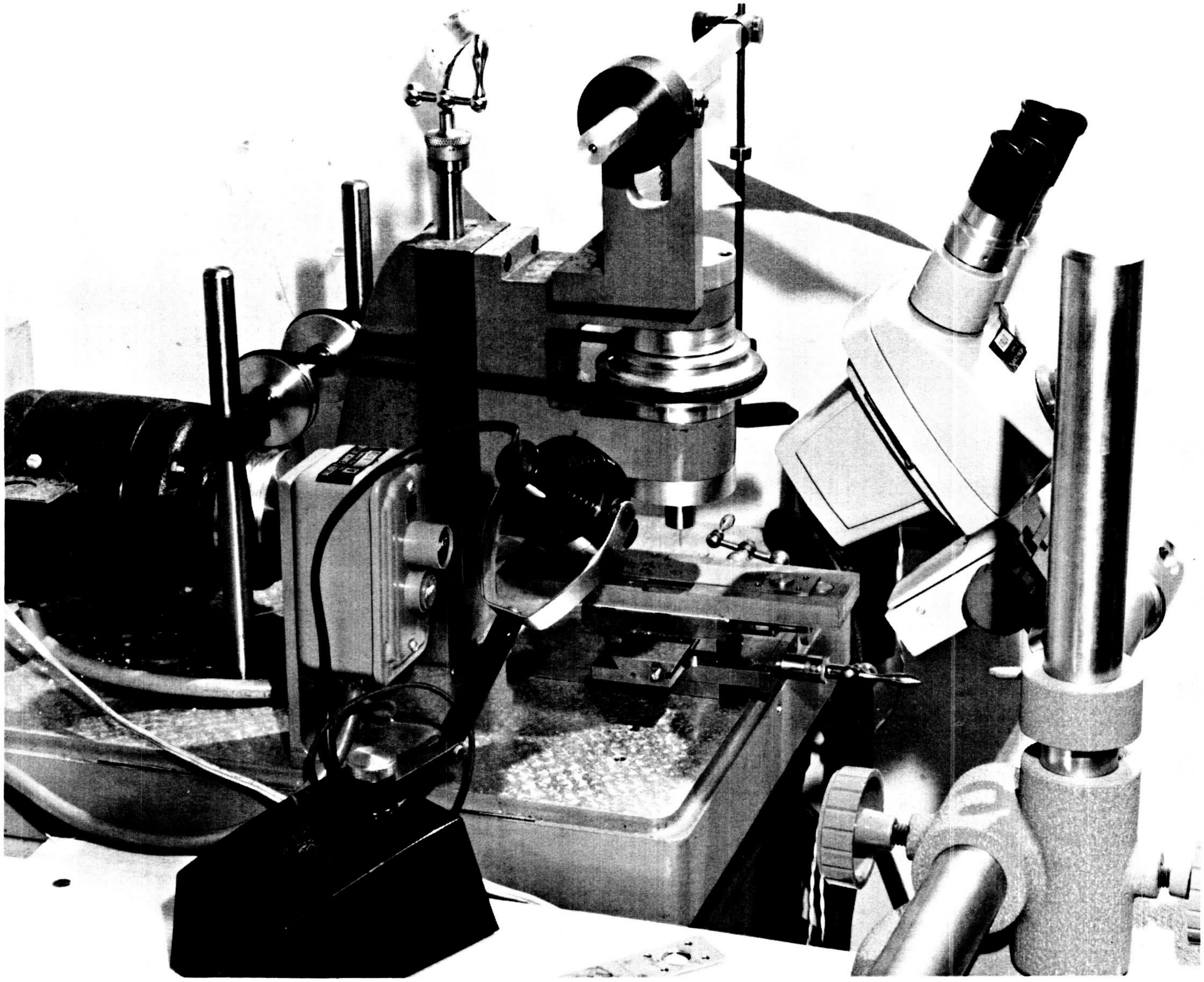

Figure 7. Micro-Drill Press and Microscope Arrangement for Drilling Notch-End Holes in Specimens.

these specimens and the specimen configurations are shown in Figs. 8, 9, and 10.

The choice of width dimensions in ultimate tensile strength specimens can be critical if the σ_{tu} values are to be used in notch strength calculations. Gerard (6) analyzed fracture strains and found that equivalent behavior occurred when the width of a smooth tensile specimen was the same as the width of a single ligament in an internally notched tensile specimen. In accordance with these findings, all the smooth tensile specimens were manufactured with a width of 0.300 in. (7.62 mm) which corresponds to the single ligament width of the notched specimen shown in Fig. 6.

Short gage length specimens shown in Fig. 8 were tested to obtain ultimate strength data and for stress-strain properties. For the latter, pairs of BLH foil strain gages Type FAP-25-12 were applied back-to-back on the gage section and connected to eliminate bending response.

Two-inch permanent strains after fracture were obtained from measurements of gage marks on the long gage length specimens shown in Fig. 9. Machine shop layout-compound was first applied on the specimen surface and light gage marks were carefully scratched through the surface coat with a precision height gage at 0.500 in. (12.70 mm) intervals along the gage length. Care was taken to penetrate only through the coating, this leaving the metal surface virtually unmarred. After fracture the specimens were fitted together and the gage distances were measured using an optical comparator.

We planned to measure small gage length strains using a photogrid consisting of 0.002 in. (0.05 mm) width alternate clear and opaque bands. One 0.004 in. (0.10) wave length on this grid would be the gage length for the measurements. There is some difficulty applying such a grid over a large area and because of the uncertainty of the position of the fracture in standard sheet specimens, the configuration shown in Fig. 10 was adopted. The grid was placed in the central minimum section of the specimen and extended approximately 0.5 in. (13 mm) on either side of the center.

A layer of sensitive Kodak Photo-Resist was applied to the specimen. An accurate 250 line, glass Ronchi grating served as the negative and after exposure and development the grid image was dyed. The nature of the process is such that the unexposed material is dissolved during development leaving a series of individual grid lines on the specimen rather than the continuous film of conventional photographic processes. The advantage of this technique is that very large strains can be measured with no limitation imposed by the ductility characteristics of the film.

Photographs of the grids were taken using a specially constructed optical bench before and after fracture at about 8 x magnification. The strain analyses were made from the photographic negatives after precise individual determinations

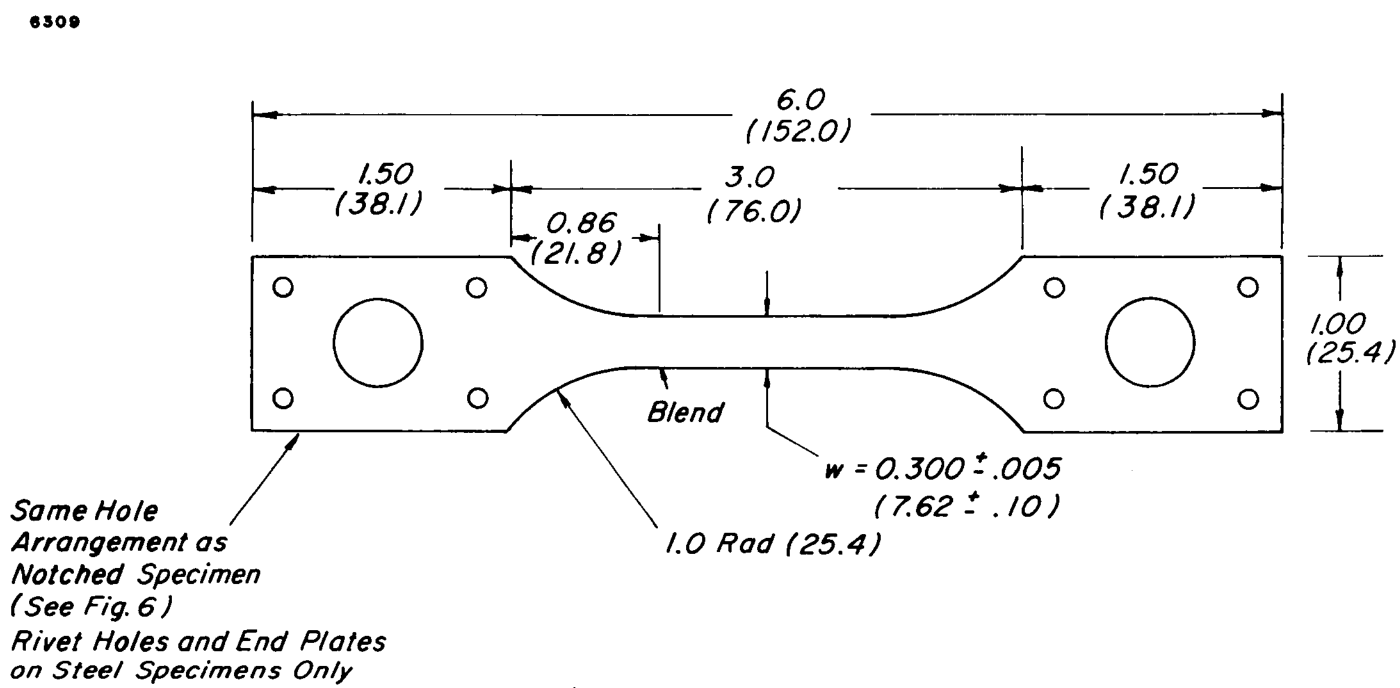

Figure 8. Sheet Tension Specimen for Stress-Strain Properties and Ultimate Tensile Strength.

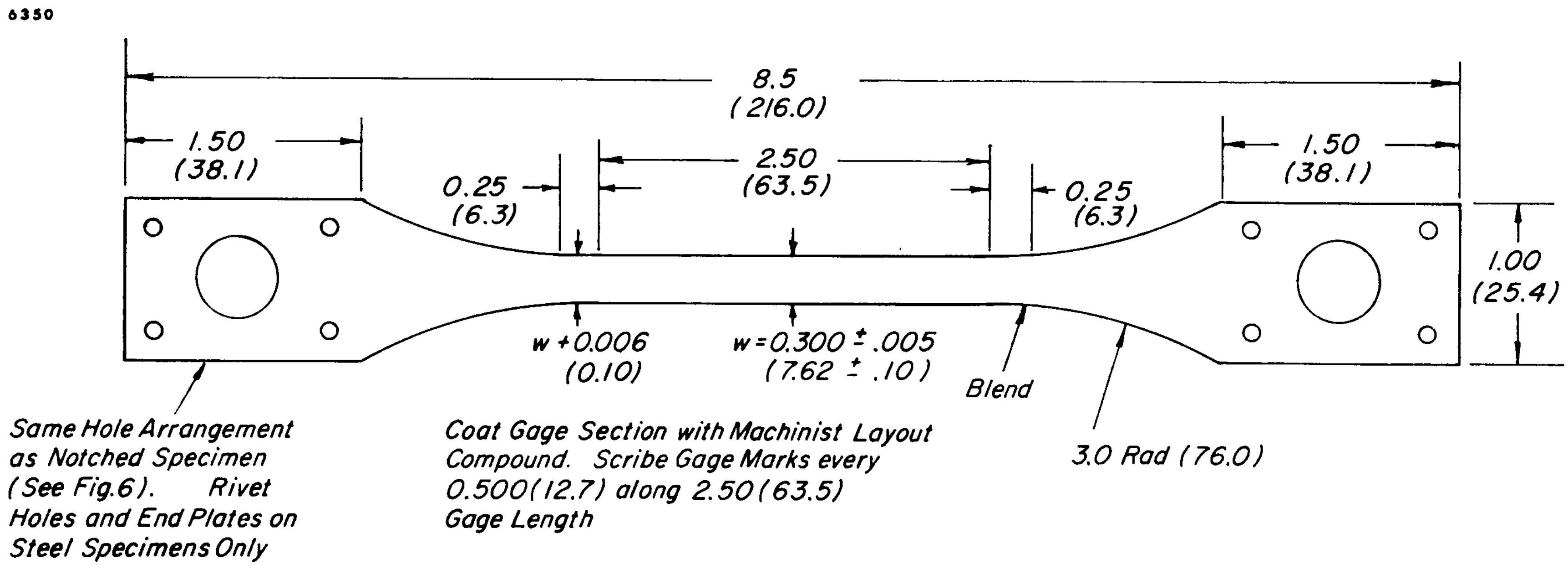

Figure 9. Sheet Tension Specimen for Two-inch Gage Length Permanent Strain Measurements.

6312

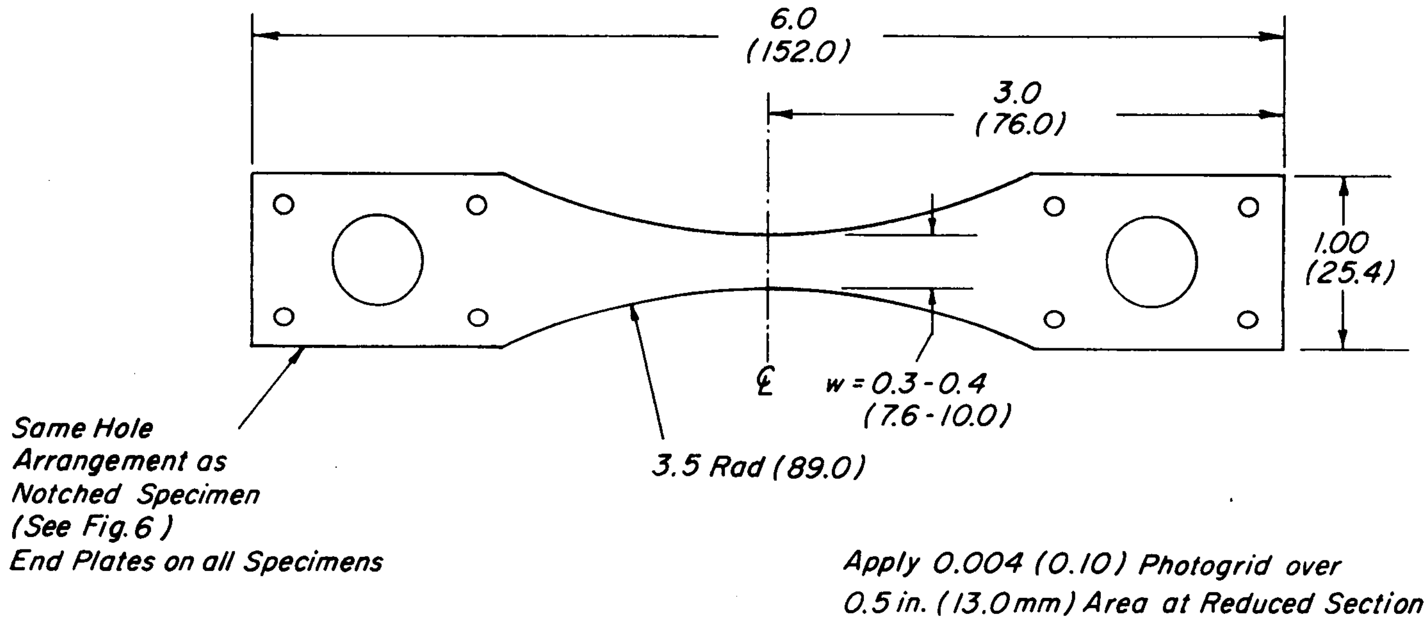

Figure 10. Sheet Tension Specimen for Zero Gage Length Strain Measurements

of the magnification on each film.

Test Technique

All specimens were loaded to fracture in an Allied Research Associates pneumatic testing machine at a constant stress rate of approximately 5 ksi/sec (35 $N/mm^2/sec.$). The machine has the characteristics of a low inertia, dead weight tester, i.e. a very soft machine, so there is little if any load drop off when large strains occur near fracture. The ultimate strength corresponding to maximum stress and the fracture strength are virtually the same in specimens tested in this machine.

Stress-strain properties were recorded autographically using the output of the strain gages and the testing machine load transducer on an X-Y recorder. In all other tests, the load was recorded as a function of time on the recorder and maximum loads were obtained from the autographic records.

The testing machine was calibrated prior to the test program using a proving ring whose own calibration was traceable to the National Bureau of Standards. The maximum error in load was estimated to be less than 0.5% for the tests. The accuracy of the stress-strain properties is limited also by the stated $\pm$ 1% error in the gage factor of the strain gages.

4. Experimental Data and Discussion

Test results in this section are presented separately for each of the two materials. This data presentation is followed by a general discussion of the test results. The results of a metallographic investigation of both materials is presented in the next section. Distinct differences in mechanical properties were observed in the steel data between the longitudinal and transverse directions and lesser directional differences in the titanium data. Because of this anisotropy, data for the longitudinal and transverse directions were analyzed separately for both materials.

A. Data for Aged Titanium Alloy Ti-6Al-4V

Ultimate Tensile Strength

Reference values of ultimate tensile strength for use in computing the plastic stress concentration factor k_p, are given in Table 4. Separate average values for each direction were used in the computation according to the relation, k_p = ultimate tensile strength/notched tensile strength.

Included in Table 4 are data for all specimens in the three configurations shown in Figures 8, 9, and 10.

Table 4. Ultimate Tensile Strength of Aged Titanium Alloy Ti-6Al-4V

Specimen No.	Orientation	Type: Figure No.	Ultimate Strength, σ_{tu} ksi	Ultimate Strength, σ_{tu} N/mm^2	Average σ_{tu} ksi	Average σ_{tu} N/mm^2
TEL-14	L	8	178	1225		
TFL-12	L	8	171	1178		
TEL-3	L	8	165	1137	173	1191
THL-2	L	9	178	1225		
TGL-3	L	9	175	1205		
THL-4	L	10	172	1184		
TFT-2	T	8	170	1170		
TFT-12	T	8	163	1122		
TFT-11	T	8	161	1109	166	1142
THT-3	T	9	168	1157		
TGT-1	T	9	169	1164		
TGT-3	T	10	167	1150		

Notch Strength

The notch strength data and concentration factors are given in Table 5 for the longitudinal direction and Table 6 for the transverse direction. Given in the appendix are specimen dimensions in Tables A1 and A2 and photographs of typical fractured longitudinal and transverse specimens in Fig. A1. All fractures were in shear either in the plane of the sheet or through the thickness. Some included a combination of these conditions. Values of the elastic concentration factor in Tables 5 and 6 were computed separately for each specimen using the measured dimensions and Eq. (9). The notch-end radii for the small diameter holes were not measured directly; rather they were taken from the dimensions of the reamer used to form the hole.

The k_p vs k_e data are shown graphically for the longitudinal and transverse directions in Fig. 11. The data appear to follow the behavior described in Eqs. (4) and (5). As a first approximation it was assumed that k_{eo} was less than 5 for both sets of data and linear least squares analyses were made using the data for $k_e > 4$ to determine the values of $\bar{e}$ in Eq. (5) and, by computation, the values of k_{eo}. The appropriately sloped straight lines have been drawn on the figure.

Two-inch Gage Length Strains

Four specimens, two longitudinal and two transverse, were tested to obtain the two-inch gage length strain values. In one of the transverse specimens, fracture occurred outside of the gage length. Data for the remaining specimens are as follows:

Longitudinal:	Spec	THL-2	7.1%
		TGL-3	7.0%
Transverse:		THT-3	4.1%
		TGT-1	Fractured outside gage length.

Small Gage Length Strains

Small gage length strains were obtained from measurements of the displacements of the grid lines on photographs of the fractured photogrid specimens shown in Fig. 12. The engineering definition of strain served as a basis for the measurements, viz. $\epsilon = \Delta L/L$. The ΔL values were obtained from the axial component of displacement of the grid lines on the grid photographs, taking into account the magnification of the grid images. Measurements were made on an optical comparator whose least count was 0.0001 in. (0.0025 mm) which is the equivalent of 3% strain. Measurements were made along the fractured edges on both halves of each of two fractured specimens (one L and one T). The strain vs position data are shown in Fig. 13.

Table 5. Notch Strength Test Results for Aged Titanium Alloy Ti-6Al-4V in the Longitudinal Direction

Specimen No.	Notch-End Radius, r in	mm	k_e	Notch Strength ksi	N/mm^2	k_p*
TFL-21	0.0625	1.59	2.99	176	1211	0.98
TFL-9	0.0625	1.59	2.99	171	1178	1.01
TFL-19	0.0625	1.59	2.99	166	1143	1.04
TEL-4	0.0312	0.79	3.99	165	1136	1.05
TEL-15	0.0312	0.79	3.99	180	1240	0.96
TFL-11	0.0312	0.79	3.98	171	1178	1.01
TFL-17	0.0180	0.46	5.02	167	1150	1.04
TEL-17	0.0180	0.46	5.03	176	1211	0.98
TFL-10	0.0180	0.46	5.02	168	1157	1.03
TEL-1	0.0180	0.46	5.03	166	1143	1.04
TEL-9	0.0120	0.30	6.02	166	1143	1.04
TEL-13	0.0120	0.30	6.01	166	1143	1.04
TFL-20	0.0120	0.30	6.02	161	1109	1.07
TFL-16	0.0087	0.22	6.96	156	1073	1.11
TFL-18	0.0087	0.22	6.96	163	1122	1.06
TFL-8	0.0087	0.22	6.96	167	1150	1.04
TEL-20	0.0064	0.16	7.97	168	1157	1.03
TEL-8	0.0064	0.16	7.99	163	1122	1.06
TEL-19	0.0064	0.16	7.98	162	1116	1.07
TEL-18	0.0049	0.12	9.01	158	1088	1.10
TEL-11	0.0049	0.12	9.03	159	1095	1.09
TFL-7	0.0049	0.12	9.01	160	1102	1.08
TEL-16	0.0040	0.10	9.94	156	1073	1.11
TEL-12	0.0040	0.10	9.94	152	1048	1.14
TEL-10	0.0040	0.10	9.97	156	1073	1.11
TFL-4	0.0033	0.08	10.85	159	1095	1.09
TFL-14	0.0033	0.08	10.85	156	1073	1.11
TEL-5	0.0028	0.07	11.85	153	1054	1.13
TFL-5	0.0028	0.07	11.85	156	1073	1.11
TFL-6	0.0023	0.06	12.89	155	1068	1.12
TEL-6	0.0023	0.06	12.90	153	1054	1.13
TFL-2	0.0021	0.05	13.45	146	1005	1.18
TEL-2	0.0021	0.05	13.46	152	1047	1.14

*Reference value of ultimate tensile strength, σ_{tu} = 173 ksi (1191 N/mm^2).

Table 6. Notch Strength Test Results for Aged Titanium Alloy Ti-6Al-4V in the Transverse Direction

Specimen No.	Notch-End Radius, r in	Notch-End Radius, r mm	k_e	Notch Strength ksi	Notch Strength N/mm^2	k_p*
TET-1	0.0625	1.59	2.99	163	1122	1.02
TFT-6	0.0625	1.59	2.99	167	115	0.99
TFT-21	0.0625	1.59	3.02	166	1143	1.00
TFT-1	0.0312	0.79	3.98	169	1165	0.98
TFT-7	0.0312	0.79	3.98	163	1122	1.02
TFT-8	0.0312	0.79	3.98	162	1116	1.02
TET-3	0.0180	0.46	5.01	163	1122	1.02
TFT-13	0.0180	0.46	5.03	153	1054	1.08
TET-4	0.0120	0.30	6.01	159	1095	1.04
TFT-5	0.0120	0.30	6.02	165	1136	1.01
TET-2	0.0120	0.30	6.03	159	1095	1.04
TFT-15	0.0087	0.22	6.96	163	1122	1.02
TET-21	0.0087	0.22	6.96	159	1095	1.04
TFT-14	0.0064	0.16	7.98	151	1041	1.10
TFT-20	0.0064	0.16	7.98	155	1068	1.07
TFT-3	0.0064	0.16	7.99	162	1116	1.02
TFT-18	0.0049	0.12	9.02	150	1033	1.11
TFT-19	0.0049	0.12	9.00	152	1047	1.09
TET-10	0.0049	0.12	9.02	155	1068	1.07
TFT-4	0.0040	0.10	9.94	142	978	1.17
TET-6	0.0040	0.10	9.97	151	1040	1.10
TET-12	0.0033	0.08	10.85	151	1048	1.10
TET-11	0.0033	0.08	10.85	148	1019	1.12
TET-14	0.0028	0.07	11.85	147	1012	1.13
TET-13	0.0028	0.07	11.85	148	1019	1.12
TFT-16	0.0023	0.06	12.90	138	950	1.20
TET-15	0.0023	0.06	12.90	149	1027	1.19
TET-17	0.0021	0.05	13.46	143	985	1.16
TET-18	0.0021	0.05	13.46	144	992	1.15

*Reference value of ultimate tensile strength σ_{tu} = 166 ksi (1142 N/mm^2).

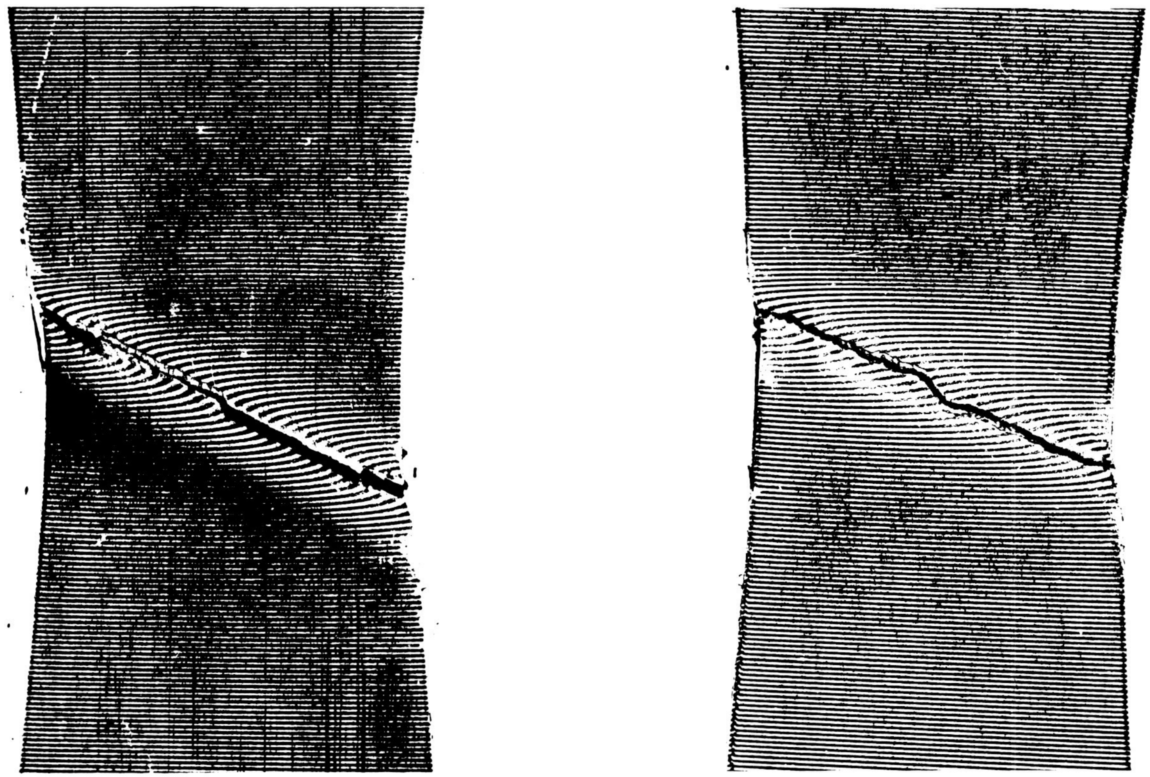

Figure 12. Grid Photographs of Fractured Specimens of Aged Titanium Alloy Ti-6Al-4V (Longitudinal-Left, Transverse-Right)

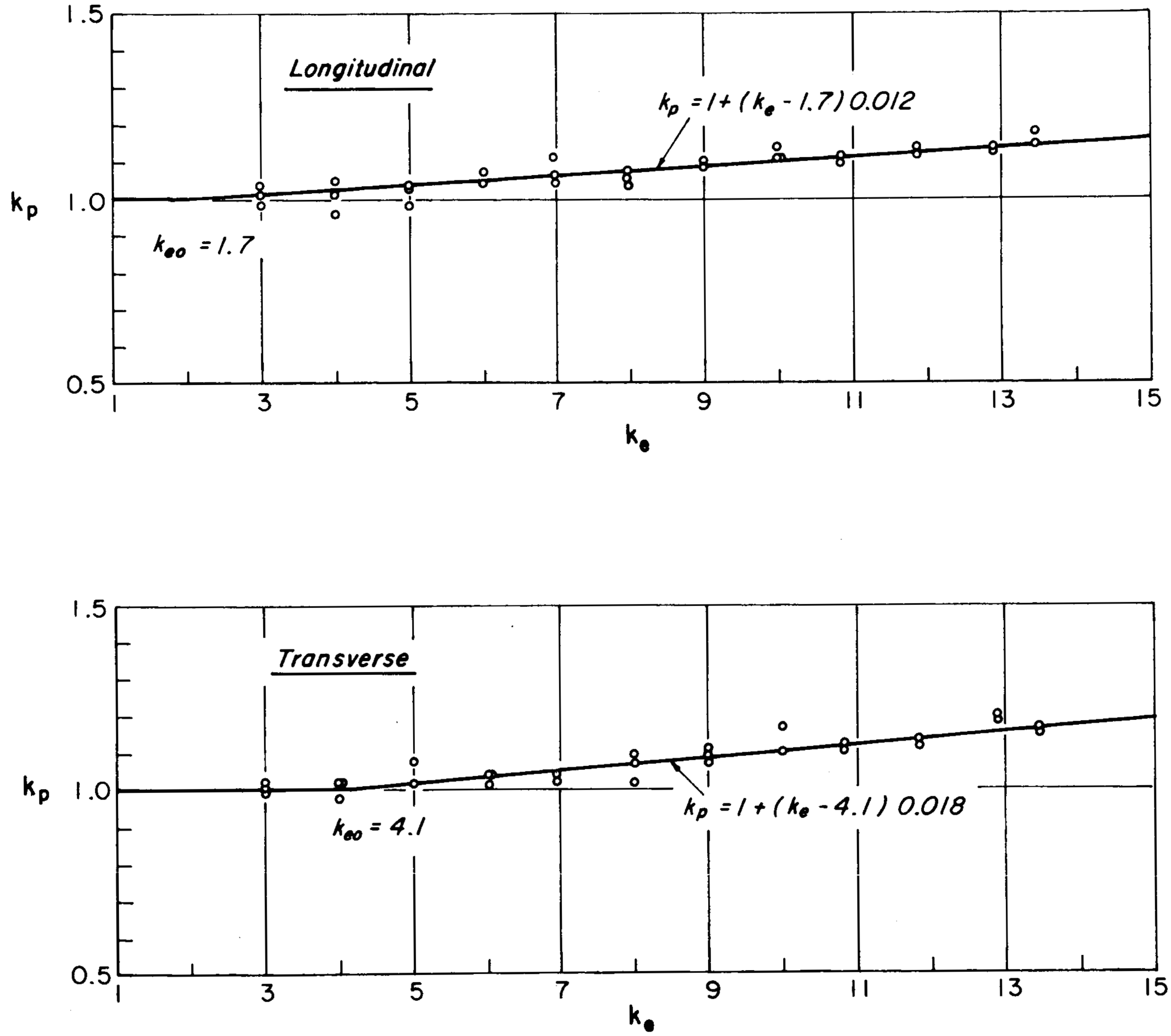

Figure 11. Elastic and Plastic Stress Concentration Data for Aged Titanium Alloy Ti-6Al-4V in the Longitudinal and Transverse Directions.

6315

6304

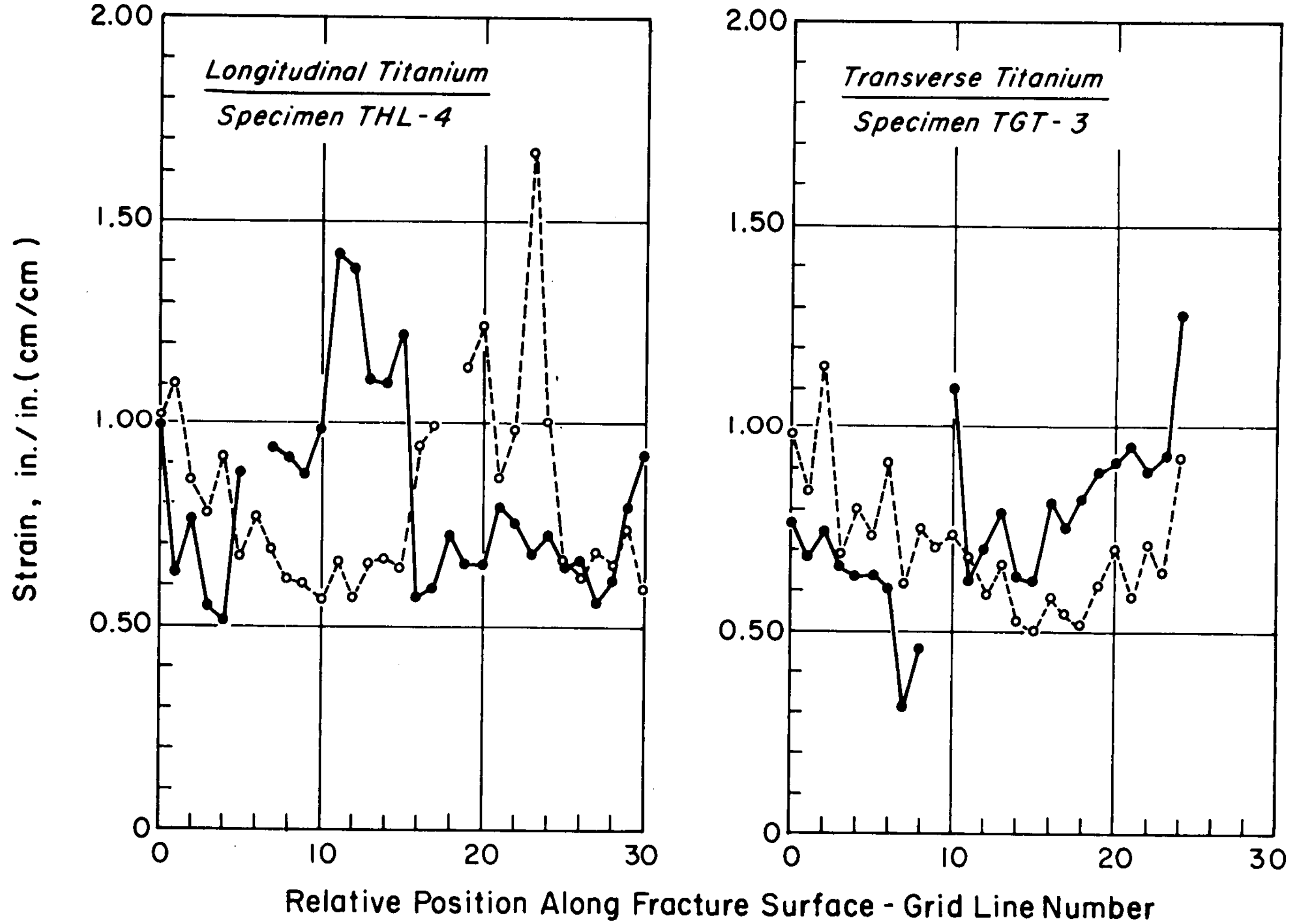

Figure 13. Small Gage Length (0.004 in. - 0.10 mm) Strains Along Fracture for Aged Titanium Alloy Ti-6Al-4V in Longitudinal and Transverse Direction Specimens - (Solid and dashed lines differentiate scans on each side of the fracture.)

Measurements of strain were also made by scans in the axial direction away from the fracture edge to determine the strain gradient in the neighborhood of the fracture and also by extrapolation to determine the zero gage length strains. Scans were made in six locations on each of the two specimens to measure the strain in the first 0.004 in. (0.10 mm) gage length at the fracture surface, then in a 0.008 in. (0.2 mm) gage length etc. and the values were averaged for each specimen. The averaged data are presented in Fig. 14 together with the extrapolated zero gage length values.

Stress-Strain Data

Stress-strain curves for the two directions are given in Fig. 15 with the pertinent modulus, yield strength, and ultimate strength data entered on the figure.

B. Data for Aged 18% Nickel Maraging Steel (250)

The data collected for the steel material was exactly analagous to that for titanium. The details of data collection which were given for the titanium material also apply to the steel and will not be repreated. The pertinent data themselves are given below.

Ultimate Tensile Strength

The data from specimens of various configurations are given in Table 7 on page 29.

6317

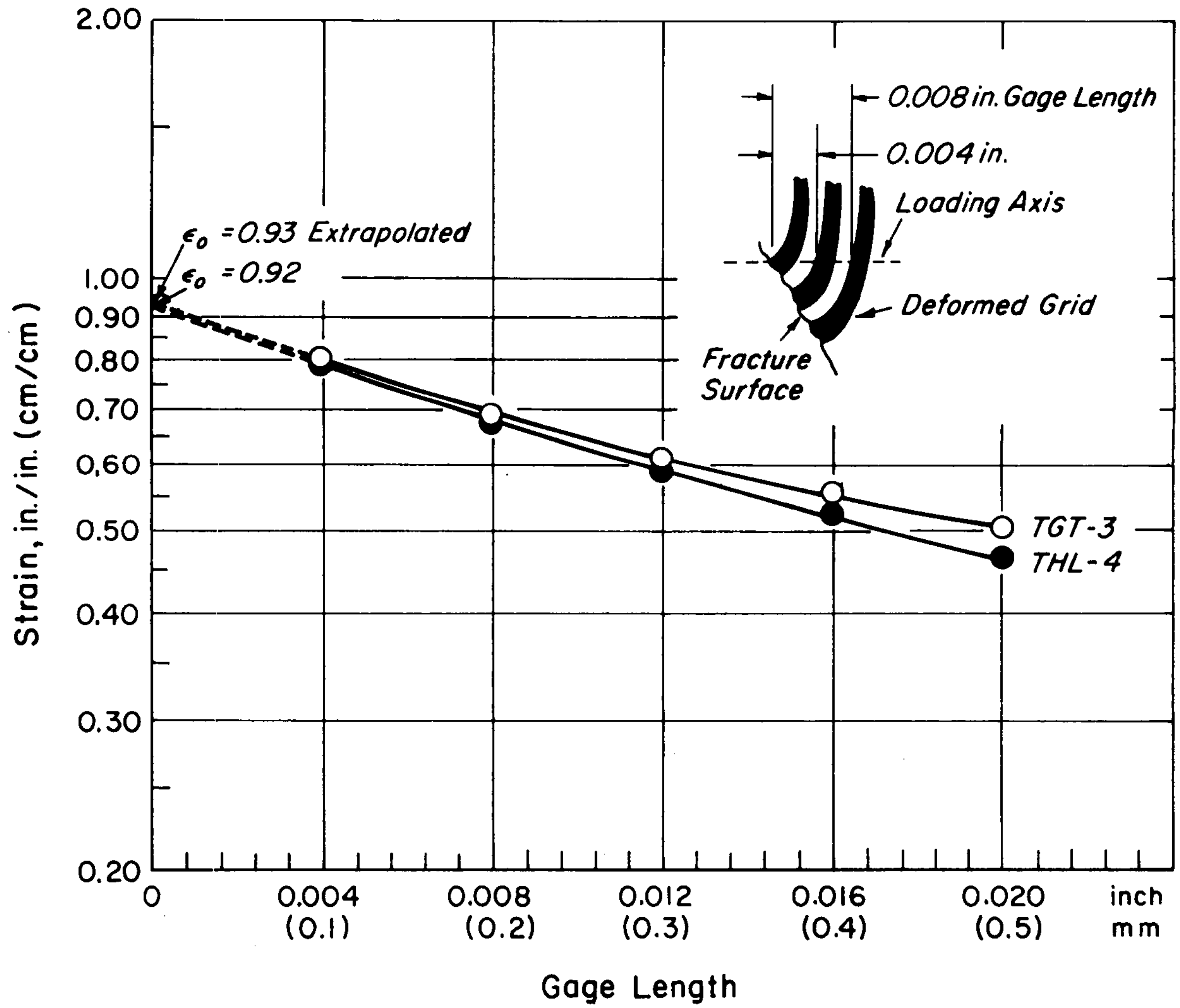

Figure 14. Strain as a Function of Gage Length in the Fracture Zone for Aged Titanium Alloy Ti-6Al-4V - Longitudinal and Transverse Directions.

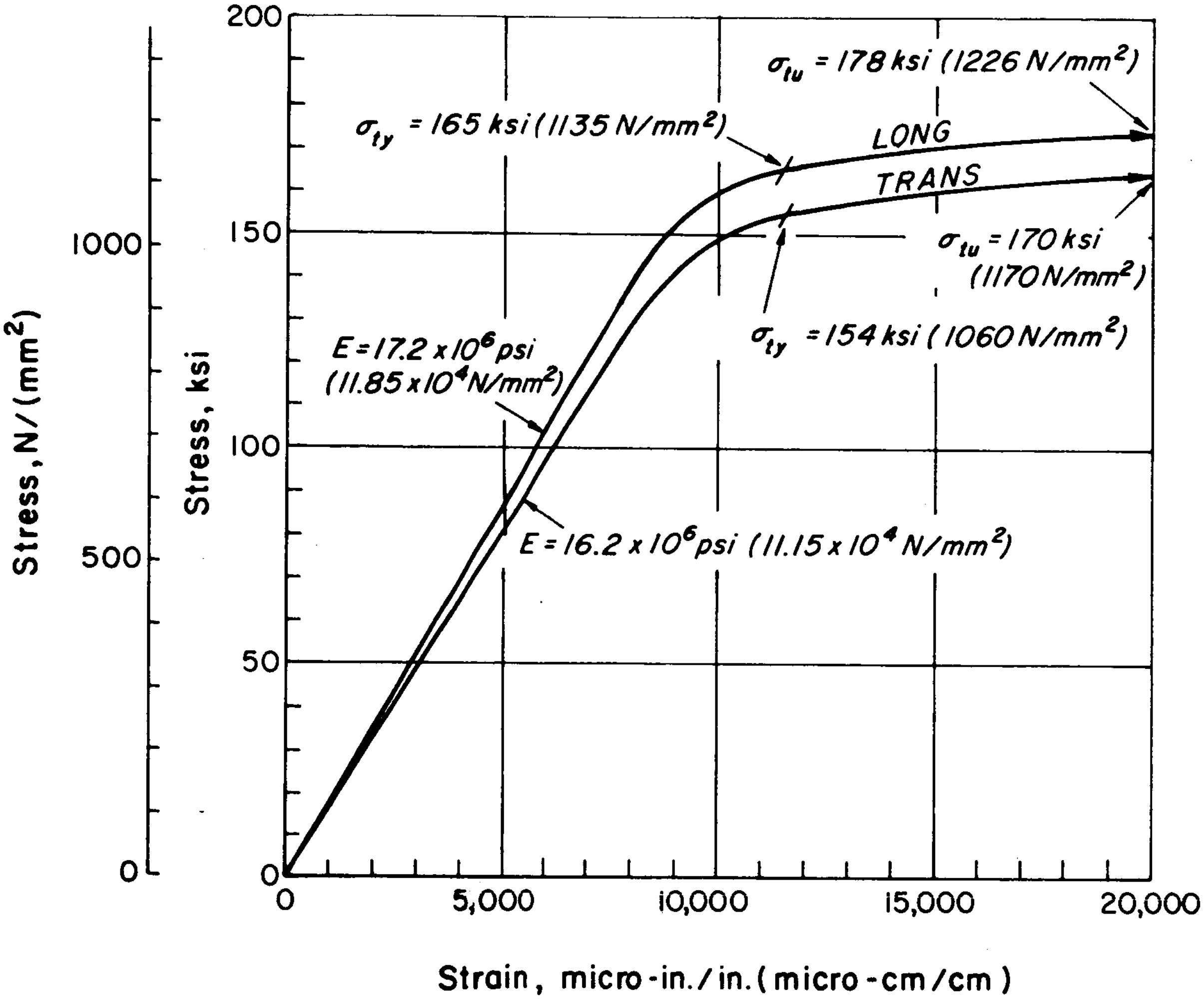

Figure 15. Stress-Strain Properties of Aged Titanium Alloy Ti-6Al-4V in the Longitudinal and Transverse Directions.

Table 7. Ultimate Tensile Strength of Aged 18% Nickel Maraging Steel

Specimen No.	Orientation	Type: Figure No.	Ultimate Strength, σ_{tu} ksi	Ultimate Strength, σ_{tu} N/mm^2	Average σ_{tu} ksi	Average σ_{tu} N/mm^2
SBL-2	L	8	266	1832		
SAL-13	L	8	262	1806		
SGL-6	L	9	257	1771	263	1812
SHL-5	L	9	257	1771		
SGL-3	L	10	274	1888		
SAT-14	T	8	272	1873		
SAT-13	T	8	268	1847		
SFT-1	T	8	267	1839		
SGT-1	T	8	266	1832	269	1853
SFT-2	T	8	263	1812		
SHT-7	T	9	270	1860		
SGT-8	T	9	264	1819		
SHT-2	T	10	278	1915		

Notch Strength

Notch strength data and elastic and plastic concentration factors are given in Table 8 for the longitudinal specimens and in Table 9 for the transverse specimens. Given in the appendix are specimen dimensions in Tables A3 and A4 and photographs of typical longitudinal and transverse fractured specimens in Fig. A2. All fractures were in shear either in the plane of the sheet or through the thickness. In the longitudinal direction the shear fractures were predominately in the plane of the sheet while in the transverse direction they were through the thickness. Graphical k_p vs k_e data are given in Fig. 16 together with the least squares data for $\bar{e}$ and k_{eo} for the transverse direction. In the longitudinal direction the material appears to be insensitive to stress concentrations to values of $k_{eo} > 11$. The data for the highest elastic stress concentration factors in the range $12 \leq k_e \leq 13.4$ show some notch sensitivity. However, there are insufficient data to perform a least squares analysis to obtain a value of $\bar{e}$.

Two-inch Gage Length Strains

Data for four specimens is as follows:

Longitudinal:	Specimen	SHL-5	2.6%
		SGL-6	3.1%
Transverse:		SGT-8	2.1%
		SHT-7	1.5%

Small Gage Length Strains

The 0.004 in. (0.10 mm) gage length permanent strains along both sides of the fracture were obtained from the grid photographs in Fig. 17 are shown in Figs. 18 and 19. Strain data taken from six axial scans in the fracture zone for a longitudinal and transverse specimen and averaged are given in Fig. 20. Included in the figure are extrapolations to obtain the zero gage length strain value.

Stress-Strain Data

Stress-strain curves for the two directions are given in Fig. 21, which also includes modulus, yield strength and ultimate strength data.

Table 8. Notch Strength Test Results for Aged 18% Nickel Maraging Steel, 250 Grade in the Longitudinal Direction

Specimen No.	Notch-End Radius, r in	mm	k_e	Notch Strength ksi	N/mm^2	k_p^*
SDL-1	0.0628	1.60	2.98	263	1810	1.00
SCL-1	0.0628	1.60	2.98	270	1860	0.98
SDL-2	0.0630	1.60	2.98	268	1840	0.98
SCL-2	0.0308	0.77	3.97	270	1860	0.98
SCL-3	0.0316	0.81	3.97	268	1840	0.98
SDL-3	0.0316	0.81	3.99	271	1865	0.97
SCL-4	0.0176	0.45	5.01	271	1865	0.97
SDL-4	0.0178	0.45	5.00	269	1850	0.98
SDL-5	0.0179	0.46	5.00	266	1830	0.99
SCL-5	0.0117	0.30	6.02	272	1870	0.97
SDL-6	0.0116	0.30	6.02	268	1840	0.98
SCL-6	0.0118	0.30	6.06	270	1860	0.97
SCL-8	0.0086	0.22	6.94	265	1825	0.99
SCL-9	0.0086	0.22	6.94	268	1840	6.98
SDL-10	0.0086	0.22	6.94	266	1830	0.99
SCL-12	0.0064	0.16	7.95	264	1820	0.99
SDL-9	0.0064	0.16	7.96	255	1755	1.03
SDL-7	0.0064	0.16	7.95	266	1830	0.99
SCL-14	0.0049	0.12	9.00	259	1785	1.02
SCL-7	0.0049	0.12	9.00	261	1795	1.01
SDL-8	0.0049	0.12	9.00	265	1825	0.99
SCL-10	0.0049	0.12	9.00	265	1825	0.99
SCL-11	0.0040	0.10	9.98	261	1795	1.01
SCL-13	0.0040	0.10	9.97	261	1795	1.08
SGL-11	0.0033	0.08	10.85	263	1810	1.00
SGL-12	0.0033	0.08	10.85	263	1810	1.00
SHL-12	0.0028	0.07	11.84	262	1805	1.00
SHL-11	0.0028	0.07	11.85	253	1740	1.04
SGL-10	0.0023	0.06	12.88	254	1750	1.04
SGL-9	0.0023	0.06	12.87	259	1785	1.02
SHL-9	0.0021	0.05	13.44	252	1735	1.04
SHL-10	0.0021	0.05	13.44	257	1770	1.02

*Reference value of ultimate tensile strength σ_{tu} = 263 ksi.

Table 9. Notch Strength Test Results for Aged 18% Nickel Maraging Steel, 250 Grade in the Transverse Direction

Specimen No.	Notch-End Radius, r in	Notch-End Radius, r mm	k_e	Notch Strength ksi	Notch Strength N/mm^2	k_p*
SCT-1	0.0625	1.59	2.99	274	1890	0.98
SDT-2	0.0628	1.60	2.98	277	1910	0.97
SDT-1	0.0632	1.61	2.98	279	1920	0.96
SDT-3	0.0308	0.78	3.97	274	1890	0.98
SCT-2	0.0316	0.80	3.97	269	1850	1.00
SCT-3	0.0309	0.78	3.99	274	1890	0.98
SDT-4	0.0178	0.45	5.01	272	1875	0.99
SDT-5	0.0182	0.46	5.00	275	1895	0.98
SCT-4	0.0184	0.46	5.00	265	1825	1.02
SCT-6	0.0122	0.31	6.00	270	1860	1.00
SCT-5	0.0118	0.30	5.98	267	1840	1.01
SDT-6	0.0122	0.31	5.93	274	1890	0.98
SDT-8	0.0086	0.22	6.94	260	1790	1.03
SDT-15	0.0086	0.22	6.94	255	1760	1.05
SDT-9	0.0086	0.22	6.94	263	1810	1.02
SDT-16	0.0064	0.16	7.95	246	1695	1.09
SCT-7	0.0064	0.16	7.95	239	1650	1.12
SDT-17	0.0064	0.16	7.95	255	1755	1.05
SDT-11	0.0049	0.12	9.00	219	1510	1.23
SDT-7	0.0049	0.12	9.00	215	1480	1.25
SDT-13	0.0040	0.10	9.97	212	1460	1.27
SDT-14	0.0040	0.10	9.96	227	1565	1.18
SDT-10	0.0040	0.10	9.97	238	1640	1.13
SDT-12	0.0040	0.10	9.97	202	1390	1.33
SGT-14	0.0033	0.08	10.86	236	1630	1.14
SGT-13	0.0033	0.08	10.86	231	1590	1.16
SHT-16	0.0028	0.07	11.85	214	1475	1.26
SHT-15	0.0028	0.07	11.85	225	1550	1.19
SHT-14	0.0023	0.06	12.88	209	1440	1.28
SHT-13	0.0023	0.06	12.87	207	1425	1.30
SGT-15	0.0021	0.05	13.44	208	1430	1.29
SGT-16	0.0021	0.05	13.44	215	1480	1.25

* Reference value of ultimate tensile strength σ_{tu} = 269 ksi.

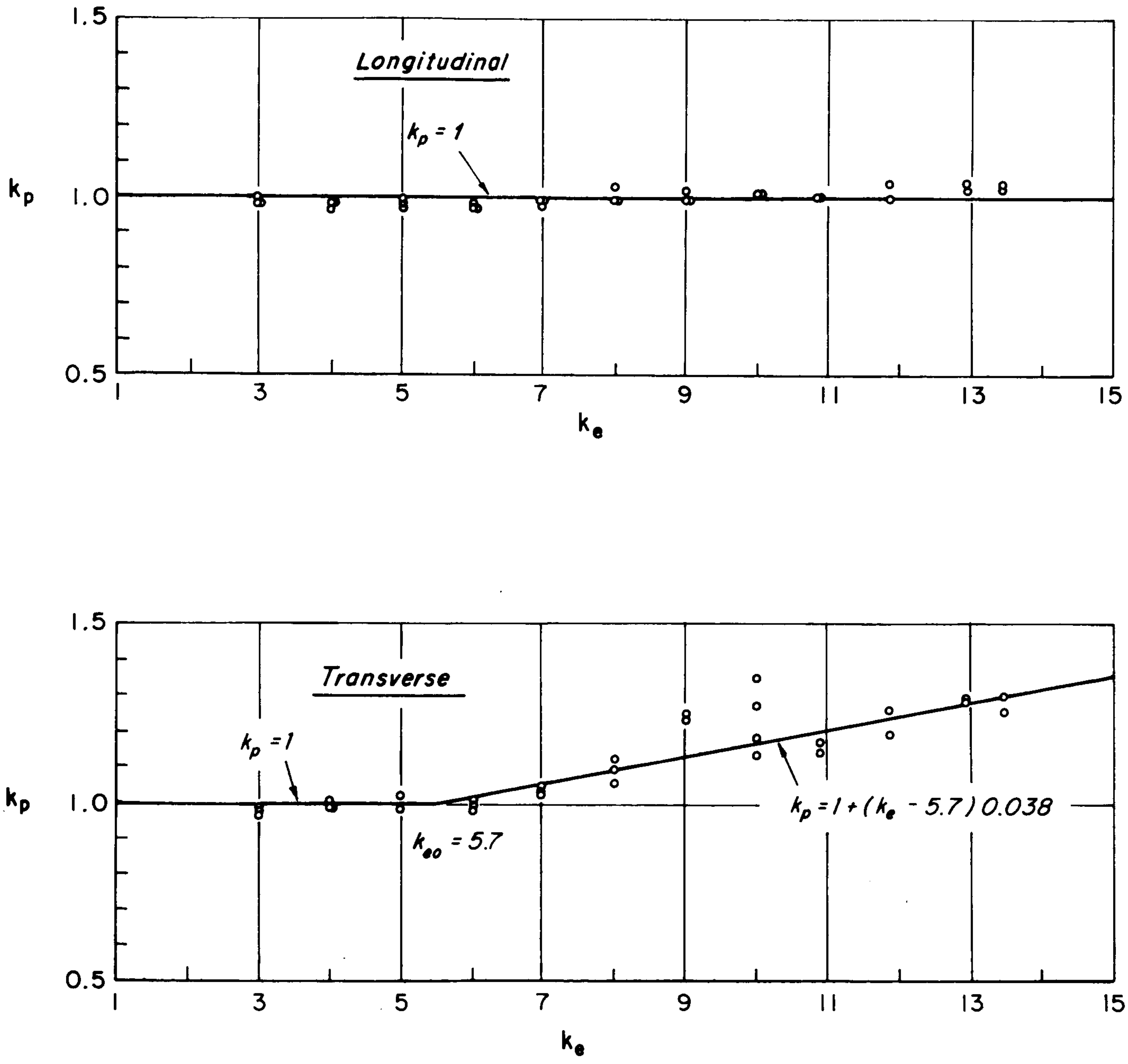

Figure 16. Elastic and Plastic Stress Concentration Data for Aged 18% Nickel Maraging Steel (250) in Longitudinal and Transverse Specimens

6314

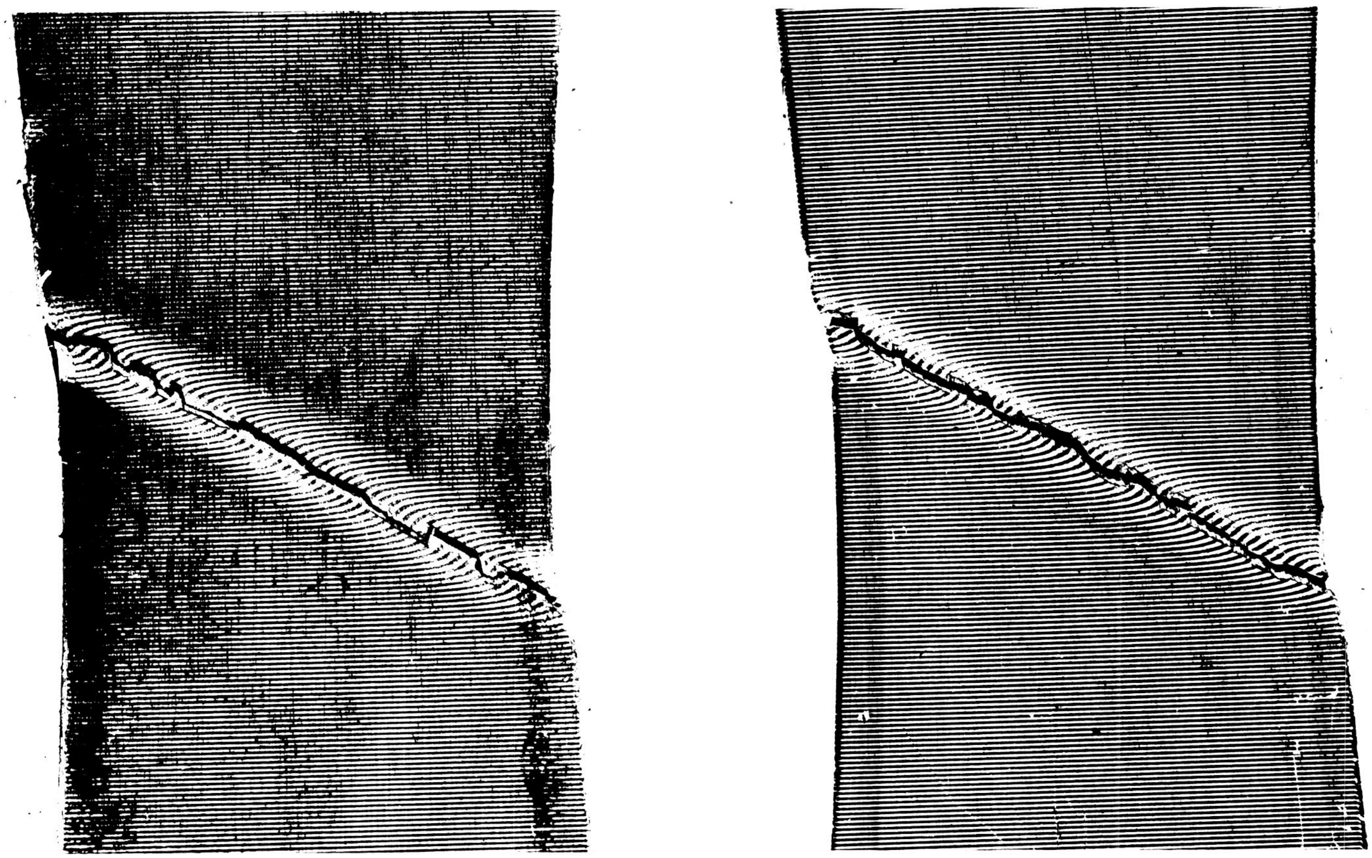

Figure 17. Grid Photographs of Fractured Specimens of Aged 18% Nickel Maraging Steel (250) - Longitudinal -Left, Transverse-Right)

6303

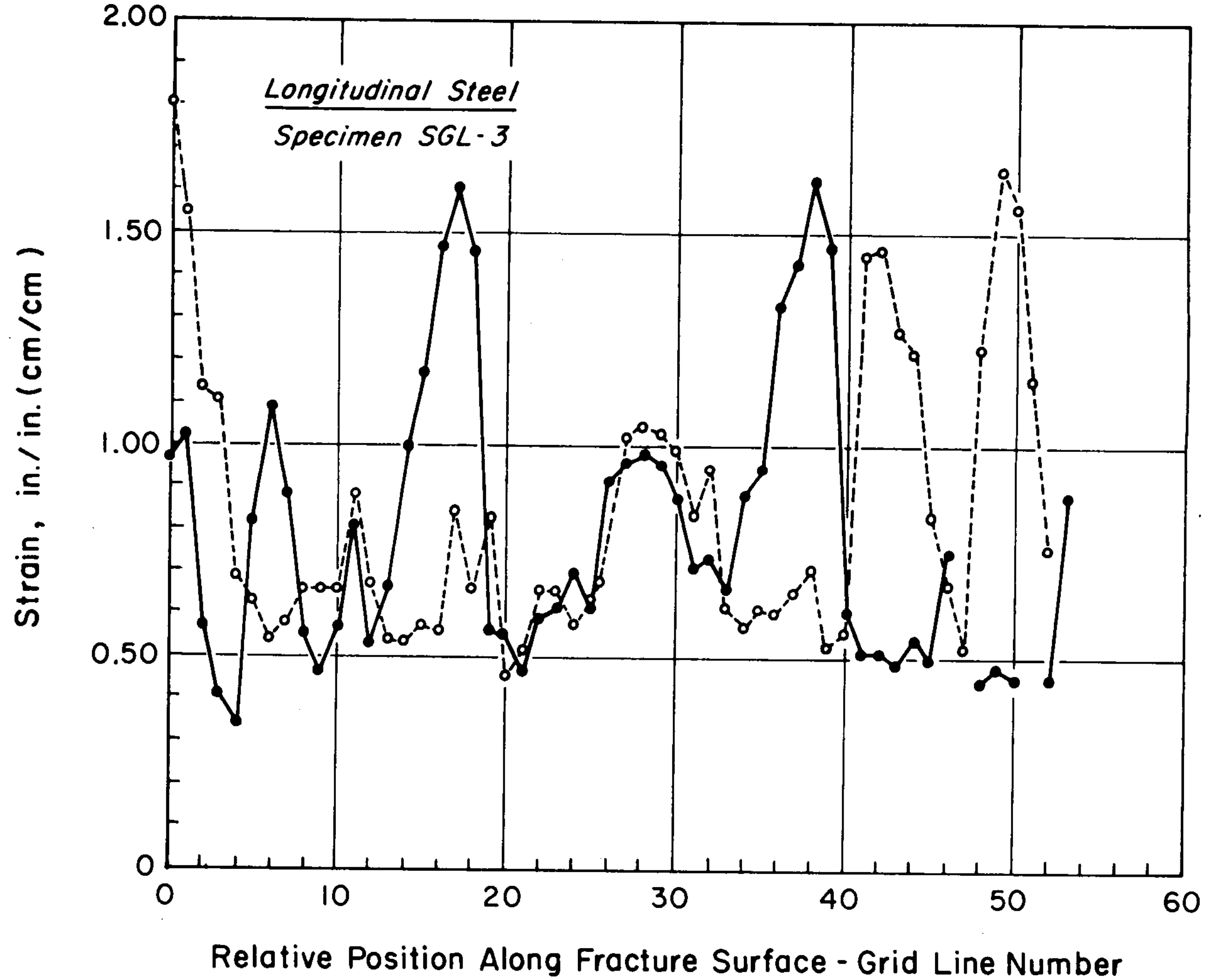

Figure 18. Small Gage Length (0.004 in. - 0.10 mm)Strains Along Fracture for Aged 18% Nickel Maraging Steel (250) - Longitudinal Direction Specimen (Solid and dashed lines differentiate scans on each side of fracture).

6267

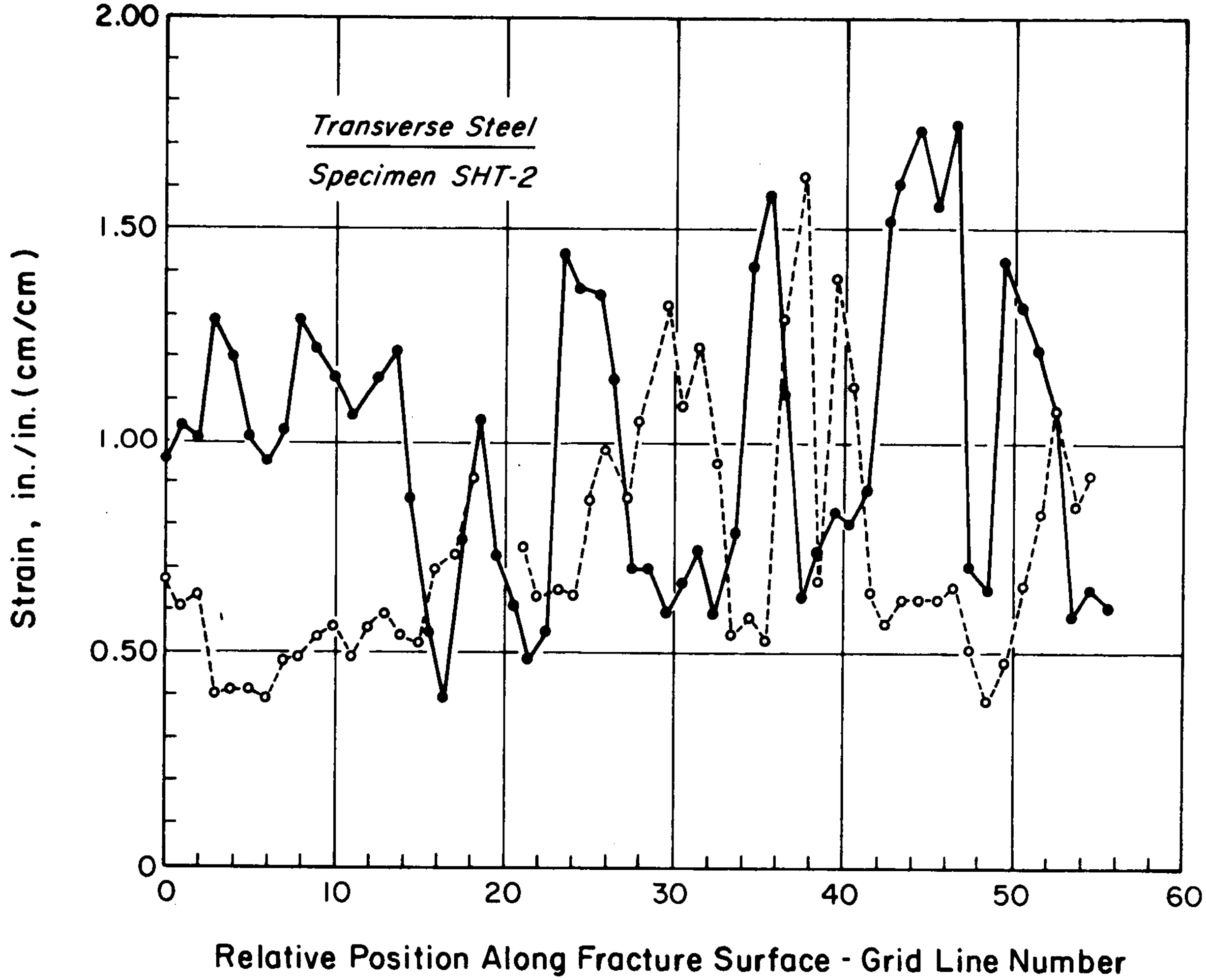

Figure 19. Small Gage Length (0.004 in. - 0.10 mm) Strains Along Fracture for Aged 18% Nickel Maraging Steel (250) - Transverse Direction Specimen (Solid and dashed lines differentiate scans on each side of Fracture).

6316

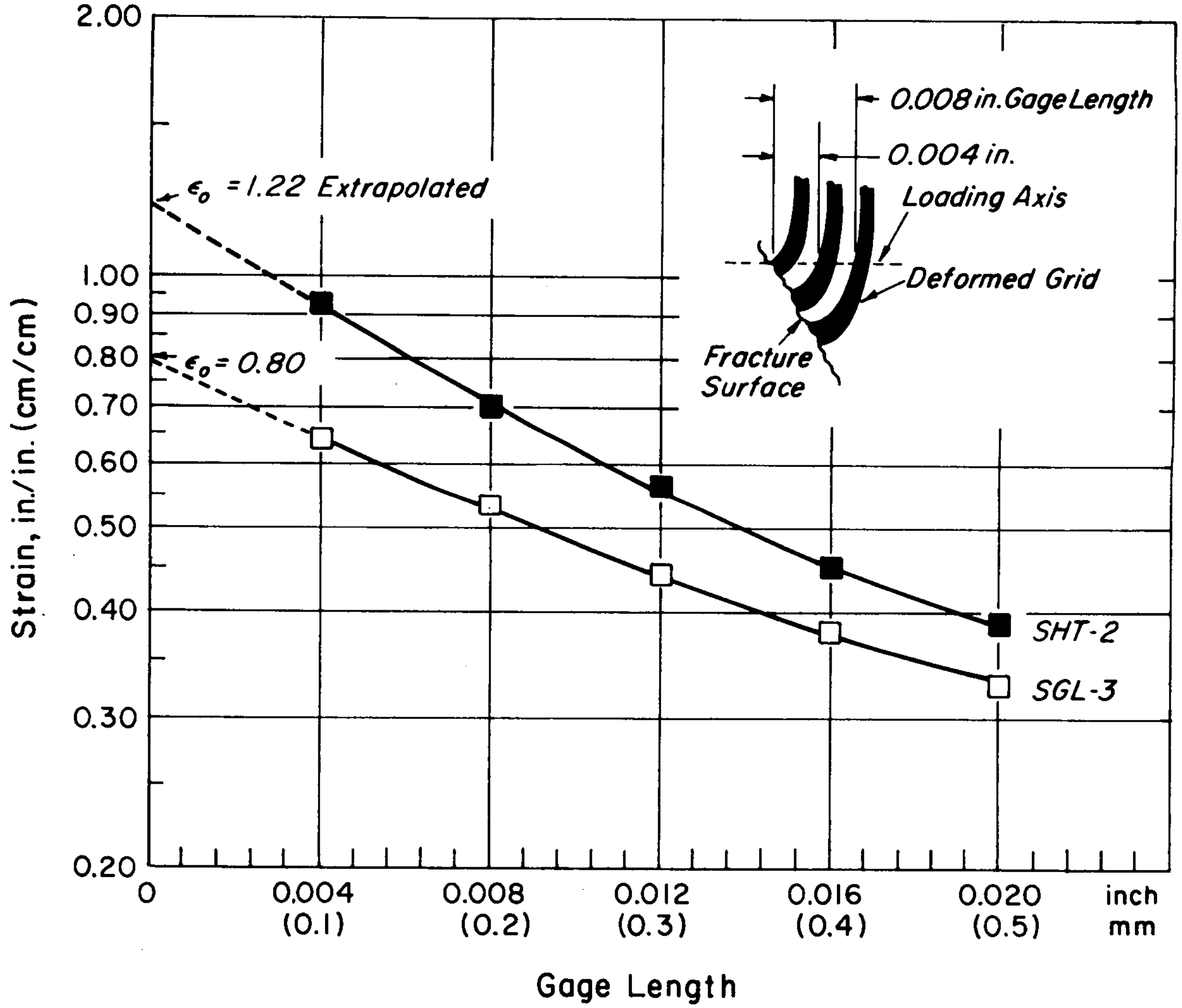

Figure 20. Strain as a Function of Gage Length in the Fracture Zone for Aged 18% Nickel Maraging Steel (250) - Longitudinal and Transverse Directions.

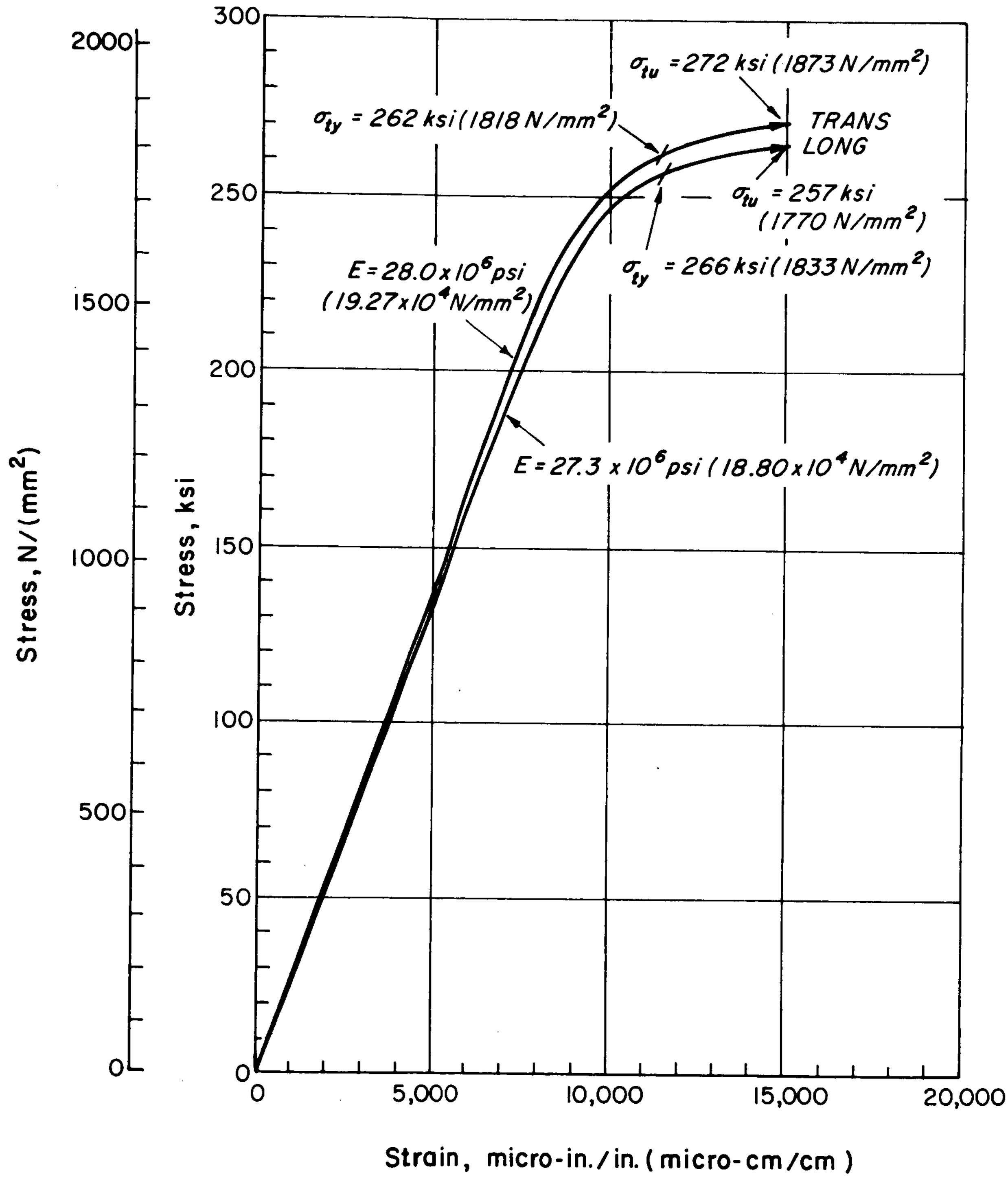

Figure 21. Stress-Strain Properties of Aged 18% Nickel Maraging Steel (250) in the Longitudinal and Transverse Directions.

6319

C. Discussion of Results

Two-inch Gage Length Strain

It is apparent from the data that the two-inch gage length strain is a very unreliable quantitative measure of structural ductility behavior. Both the titanium and the steel can be classified as limited ductility materials on the basis of exhibiting two-inch permanent strains of less than 10%, yet their sensitivity to stress concentrations is very low, approaching that of purely ductile materials. Paradoxically, the steel in the longitudinal direction with an average two-inch gage length strain of approximately 2.5% is more ductile, using the structural criterion of k_e vs k_p behavior than the titanium whose two-inch value is 4%-7%, as shown in Figs. 11 and 16.

Anisotropy

Both materials display anisotropy in mechanical behavior. In the titanium alloy the anisotropy is more evident in the stress-strain response to the yield region than in the conventional or structural ductility behavior. In the steel, however, there is relatively small anisotropy in stress-strain response but relatively large anisotropy in ductility. In both materials anisotropy in the two-inch gage length strains is mirrored in a qualitative sense by anisotropy in the k_e vs k_p structural ductility behavior. In the titanium the two-inch strains and the k_e vs k_p response may be considered isotropic while in the steel they are anisotropic. It can tentatively be concluded that anisotropy in the two-inch gage length permanent strain is an indication of anisotropy in structural ductility response.

Structural Ductility - k_e vs k_p

The results of the notch tests in both materials appear to fit the formulation given by Eqs. 4 and 5. However, since only one thickness of material was tested for each material and since only one specimen size was used, the values of k_{eo} and $\bar{e}$ found in the experiments should be considered tentative until additional tests are performed. If size effects are related to the internal grain structure of the material, we would expect that the actual specimen dimensions would have a greater influence on k_{eo} than on $\bar{e}$.

In the development of Eq. (5), it was assumed that the net section stress must be elastic in order for the ductility ratio to be constant. The stress-strains properties of both materials show that at the proportional limit, approximately $k_p = 1.25$ and that only for $k_p \geq 1.25$ is the net section stress elastic. On the other hand the

k_e vs k_p data in Fig. 11 for the Ti-6Al-4V (which exhibit relatively small scatter) appear to fit the linear relation given by Eq. (5) implying a constant ductility ratio notwithstanding the fact that all k_p values are less than 1.25. The requirement for elastic net section stress is a consequence of the original definition of the quantity e in terms of the secant modulus ratio given in Eq. (1). The results of the current investigation indicate that the analytic development of Eq. (1) should be reexamined. Since Eq. (5) is derived from Eq. (1), the latter should be considered as an empirical relation which describes structural ductility behavior.

The structural ductility parameters from Figs. 11 and 16 are summarized below:

Titanium Alloy Ti-6Al-4V:	Longitudinal	$k_{eo} = 1.7$	$\bar{e} = 0.012$
	Transverse	$k_{eo} = 4.1$	$\bar{e} = 0.018$
18% Nickel Maraging Steel (250):	Longitudinal	$k_{eo} > 11$	
	Transverse	$k_{eo} = 5.7$	$\bar{e} = 0.038$

It is interesting that significant scatter of the data occurs only in the results for the transverse direction in the steel and only for the condition $k_e > k_{eo}$. The value of ductility ratio here is also the highest ($\bar{e} =$ 0.38) of the materials tested. These results may be interpreted to mean that the scatter is due to some property of the material rather than to the conditions of the experiment. There is some metallurgical evidence to support such an interpretation as is shown in Section 5 of this report.

Small Gage Length and Zero Gage Length Strain

There have been numerous suggestions in the past that the zero gage length strain may be a fundamental measure of ductility. In order to be useful, however, such a property must have a characteristic value for each material and each condition. Our experiments with both titanium and steel show, however, that along a fracture the small gage length strains exhibit large variations in value as was shown in Figs 13, 18, and 19. We infer that the zero gage length strains would exhibit a similar variation. The variation in values for each material is clearly illustrated in Fig. 22. The longitudinal and transverse data for each material has been lumped together in the analysis; over 200 separate measurements were used for the steel and over 100 for the titanium. The variation in values extends from a minimum of approximately 30% strain to a maximum of over 170%. The titanium values are single moded with a modal value of approximately 66%. The steel distribution is bimodal with maxima at approximately 60% strain and 100% strain. As is shown in the next section, the steel structure consists of fine and coarse grain areas; the bimodal distribution may reflect differences in ductility characteristics in the two types of grain areas. Further study will be required to delineate the strain characteristics of each of the grain areas.

Although it was not possible to measure zero gage length strains at the fracture, it was possible to use an extrapolation procedure to obtain approximate values as was shown in Figs. 14 and 20. The data for the titanium show close correlation between the ϵ_o values in the two directions. The steel data show much larger variations between the two directions; this variation may be a consequence of the relatively few measurements which were made, rather than a reflection of large anisotropy. The bimodal strain distribution coupled with the observed areas of small and large grains would require many more strain scans than the six per specimen which were employed in order to obtain statistically significant numbers of strain measurements.

The ratio of zero gage length to (ϵ_o) to 0.004 in. (0.10 mm) gage length (ϵ_4) strains, however, is consistent for both directions in each material:

Titanium Ti-6Al-4V:	Longitudinal	ϵ_o/ϵ_4	= 1.16
	Transverse	ϵ_o/ϵ_4	= 1.16
18% Nickel Maraging Steel (250):	Longitudinal	ϵ_o/ϵ_4	= 1.25
	Transverse	ϵ_e/ϵ_4	= 1.28

We interpret these results as indicating that the maraging steel exhibits a steeper strain gradient in the fracture zone than the titanium alloy.

In the preceding subsection of this report we pointed out certain difficulties in correlating the secant modulus ratio concept of ductility of Eq. (1) with our k_e vs k_p data. The small gage length strain measurements reveal another difficulty. Because of the large variation in strain along the fracture there does not appear to be a characteristic value of the so called "zero" gage length strain which is specific for a material. In this case the factor E_{sm} in Eq. (1) cannot be specified except in a statistical sense and because of the large variation of strain values shown in Fig. 22 we question the use of statistically obtained values.

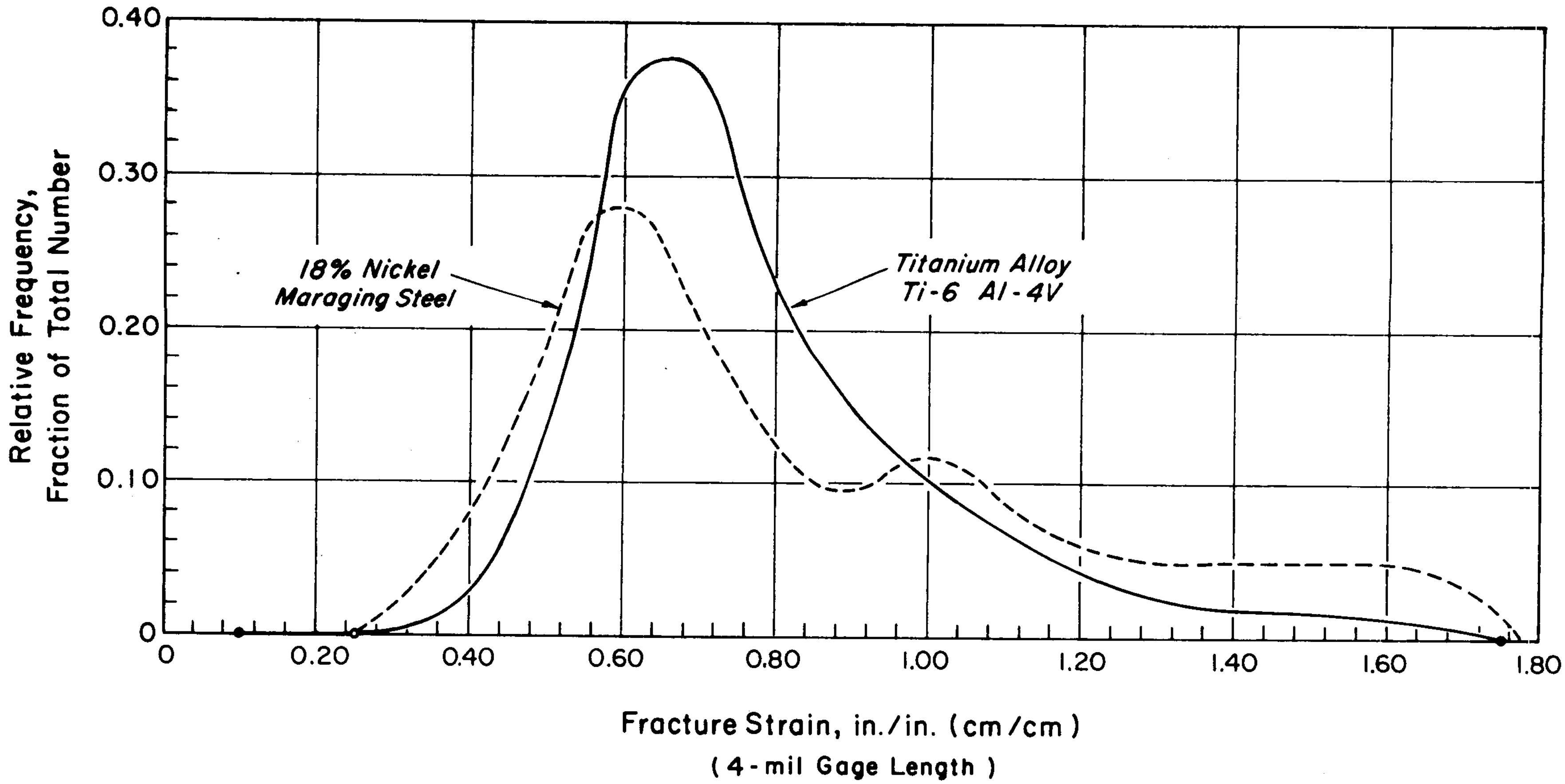

Figure 22. Frequency Distribution of 0.004 in. (0.10 mm) Gage Length Strains along the Fracture in Aged Titanium Ti-6Al-4V and Aged 18% Nickel Maraging Steel.

5. Metallurgical Studies

Metallurgical studies were made of the fracture region of a few selected tensile specimens. The purpose was to determine the possible effects of metallurgical structure on the stress-concentration factors determined from the test program. The metallurgical study was limited to the evaluation of grain size characteristics.

A. Aged Titanium Alloy Ti-6Al-4V

Fig. 23 shows the structure of a sample removed from the untested sheet supplied for the program. The microstructure appears to be the same in the plane of the sheet as in both the longitudinal and transverse cross sections with no evidence of elongated grains, except in a thin layer at the surface. The hardness taken on the sheet surface was uniform and averaged Knoop 325 (300 g), which converts to R_c32.

Fig. 24 shows the fractured longitudinal tensile specimen TET-18 used for the metallurgical studies.

Fig. 25 shows the structure along the crack path. This specimen was tested in the transverse direction and contained a stress concentration of value $k_e = 13.5$. There is slight evidence of plastic deformation at the fracture edge. The fracture appears to be transcrystalline but further study would be required to establish the validity of this conclusion. The grains appear reasonably equiaxed with fine and medium size grains uniformly distributed throughout.

On the basis of this brief study there appear to be no grain size variations in the structure of the titanium alloy sheets which would produce any appreciable metallurgical effects to cause scatter in data relating the values of k_e and k_p for values of k_e of 13.5 or less. This relatively small scatter in the data shown in Fig. 11 appears to support this observation.

B. 18% Nickel Maraging Steel (250)

The fractured tensile test specimens used for the metallurgical studies are shown in Figs. 26 and 27.

The microstructure along the crack path of the longitudinal specimen SCL-13 is shown in Fig. 28. There appears to be evidence of some plastic deformation along the crack path and at the hole surface in the region where the crack initiated. It is impossible to determine the crack path from the limited examination made. The

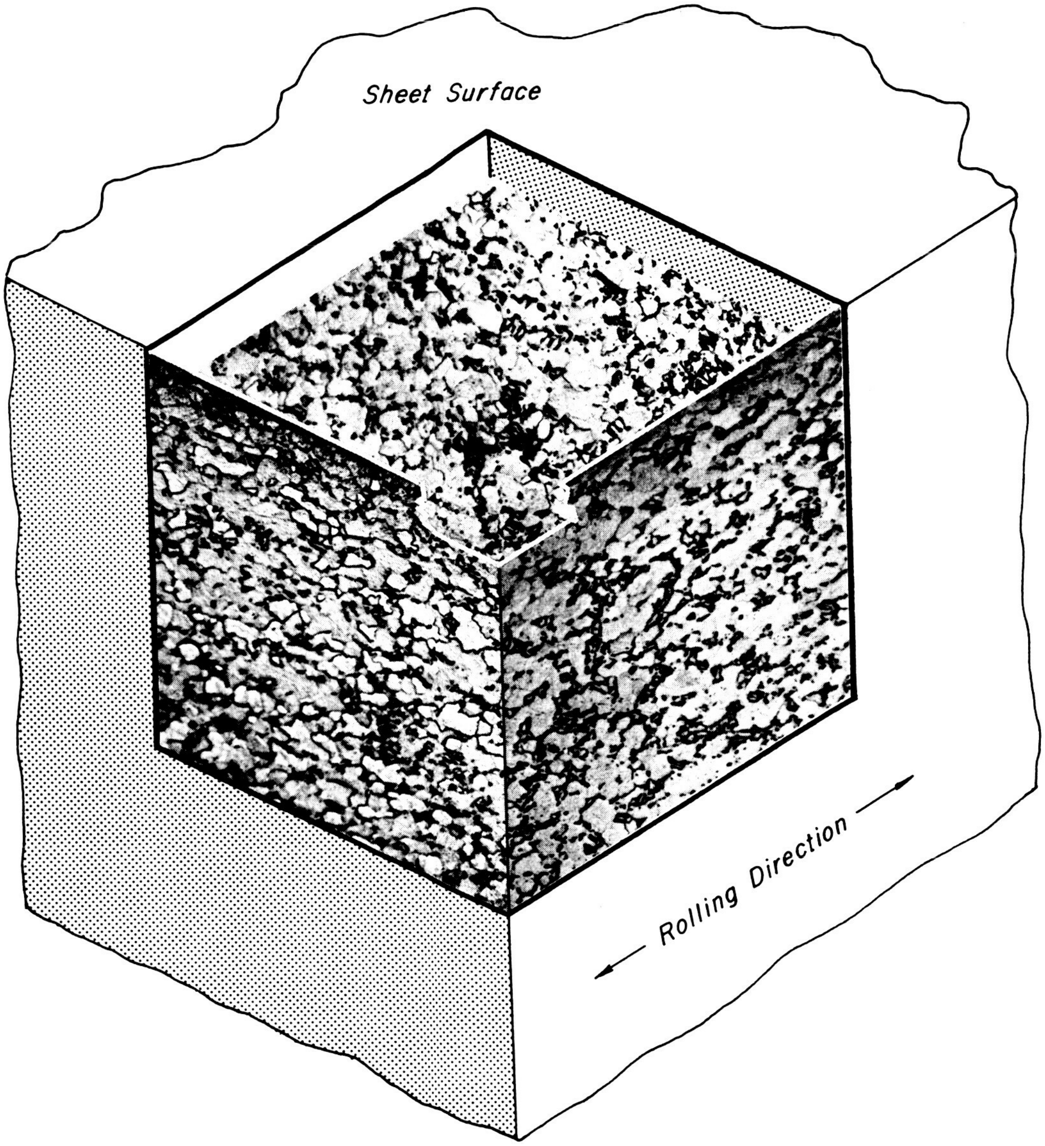

6310

Figure 23. Microstructure of Ti-6Al-4V Sheet. Magnified 500 X, Etch- Kroll's Reagent.

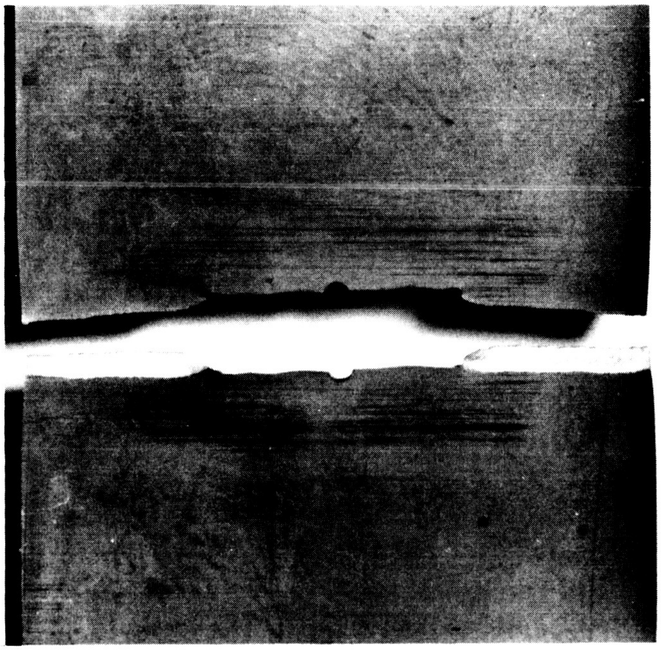

Figure 24. Fracture in Transverse Specimen TET-18 of Ti-6Al-4V Alloy (k_e = 13.5), Magnified 4.2 X.

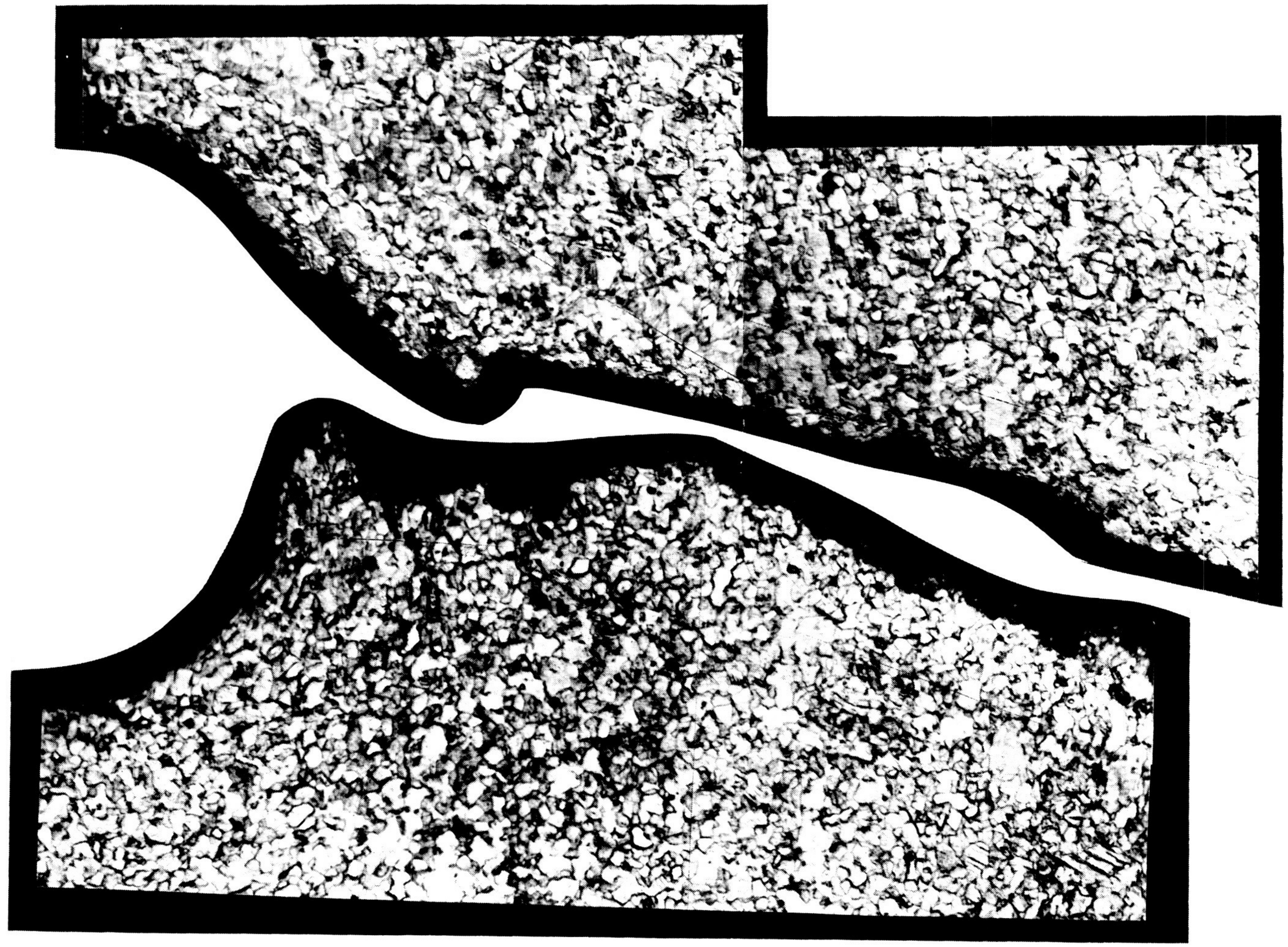

Figure 25. Section Through Fracture of Ti-6Al-4V Specimen TET-18. Magnified 500 X, Etch-Kroll's Reagent.

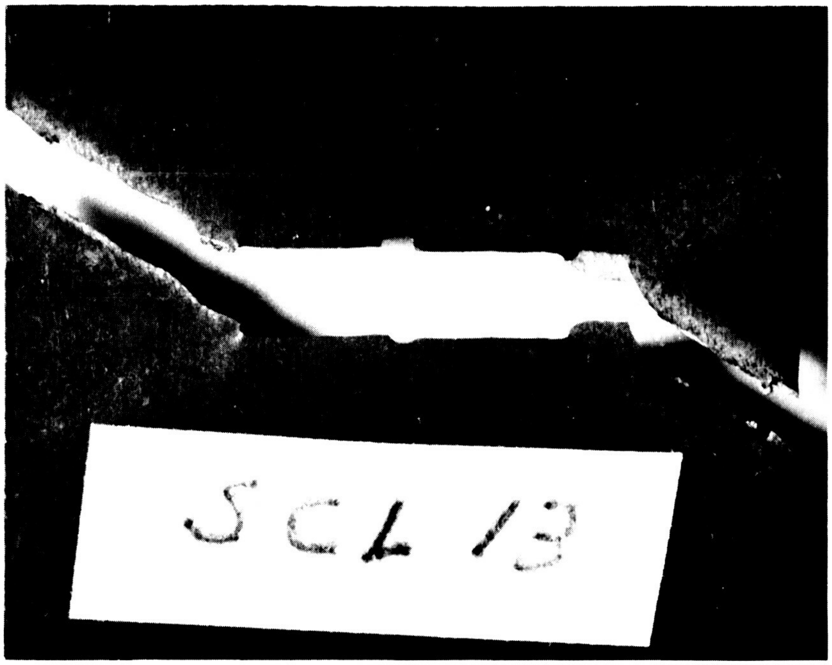

Figure 26. Fracture in Longitudinal Specimen SCL-13 of Aged 18% Nickel Maraging Steel (k_e=10). Magnified 4.2 X.

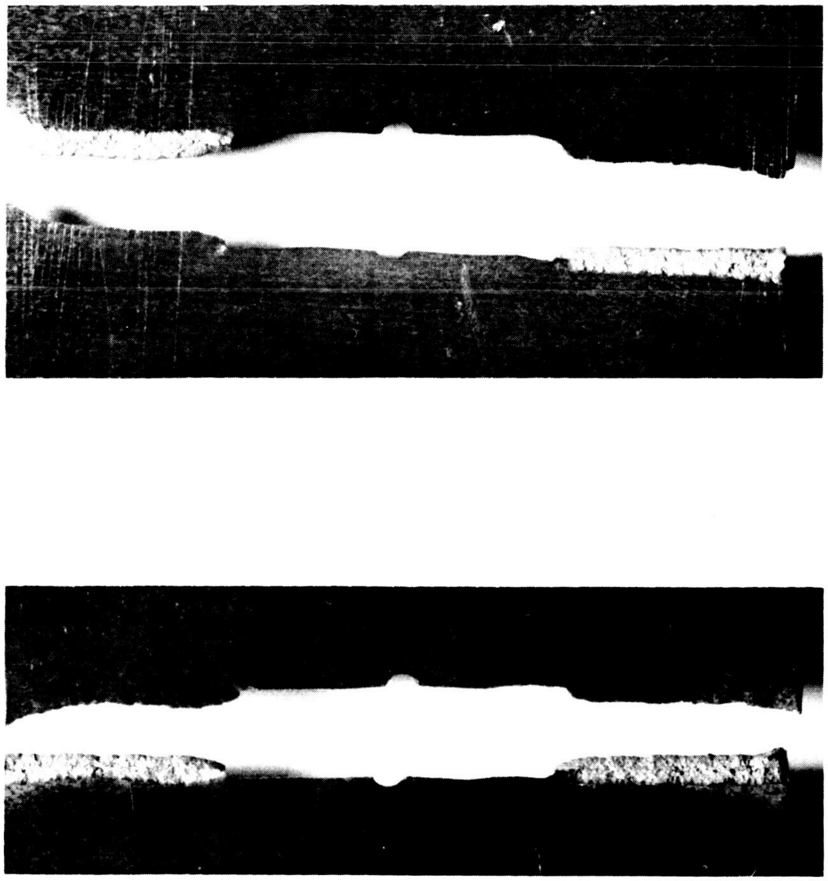

Figure 27. Fracture in Transverse Specimens SDT-12 and SDT-10 of Aged 18% Nickel Maraging Steel (k_e = 10). Magnified 4.2 X.

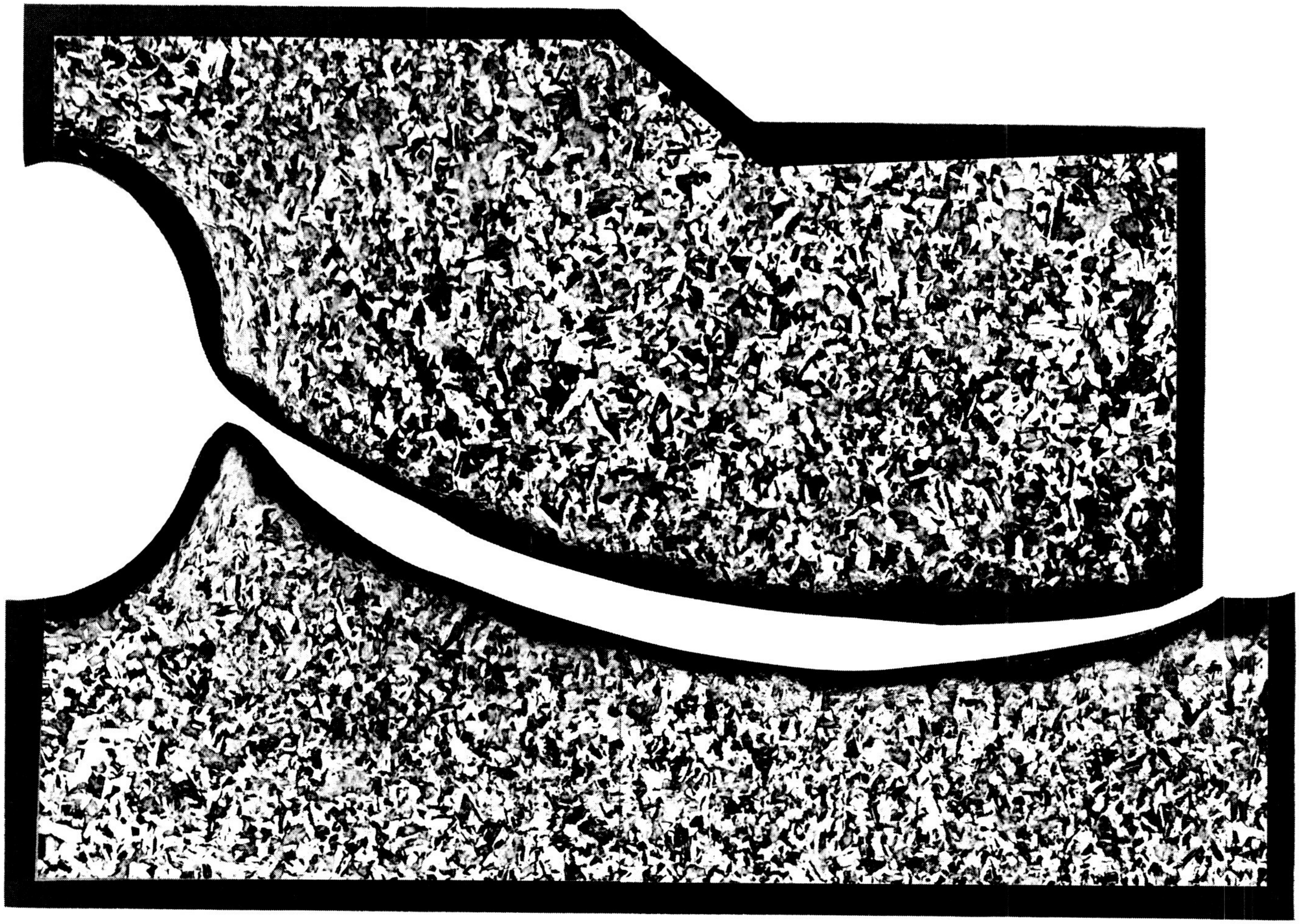

Figure 28. Section Through Fracture of Aged 18% Nickel Maraging Steel. Longitudinal Specimen SCL-13, Magnified 200 X. Etch-Fry's Reagent (Mod.).

grains in general appear undistorted and there are fine and medium size grains uniformly distributed throughout.

The microstructures along the crack paths in the transverse specimens examined are shown in Figs. 29 and 30. These specimens were chosen from the test series at a high value of $k_e = 10$, where maximum scatter in the data on k_p vs k_e occurred (See Fig. 16). Specimen SDT-10 (Fig. 29) showed a value of $k_p = 1.12$ and represents the minimum departure from $k_p = 1$. Specimen SDT-12 showed a value of $k_p = 1.31$, which was the maximum developed for the series of four specimens tested at this value of k_e.

The structure in Specimen SDT-10 (Fig. 22) shows medium to large grains with no great variation throughout. Slight plastic deformation is evident at the crack and hole edges. The structure in Specimen SDT-12 (Fig. 30) shows wide variation in grain size from rather large to extremely fine. The crack originated at the maximum stress location on the hole edge, which also happened to coincide with the coarse grain zone. The microhardness of the coarse grain region was Knoop 675 (100 g), as compared with Knoop 709 (100 g) for the fine grain zone.

The lower left section of Fig. 30 containing both coarse and fine grain areas was enlarged to 500 X. Fig. 31 shows this enlargement with arc segments drawn to scale to establish the relative size of the stress concentration holes in the specimen and the metallurgical grain structure. It is obvious that with the randomly distributed fine and coarse grain areas shown it is possible that the holes producing high stress concentrations could be entirely within either the fine or coarse area or extend from one into the other. If the properties of these areas vary, as has been shown, one would expect that the response in the tensile test would also vary depending upon where within this metallurgical structure the hole was placed.

From Fig. 31 it is difficult to determine the maximum hole size which might result in these variations for the specific metallurgical structures shown. It is obvious that for $k_e = 3$ and possibly $k_3 = 5$ the effect would not be present and for $k_e = 13.4$ and $k_e = 10$ it definitely would be. The fact that test data in Fig. 16 indicates scatter above a k_e of about 6.5 is not inconsistent with the metallurgical data.

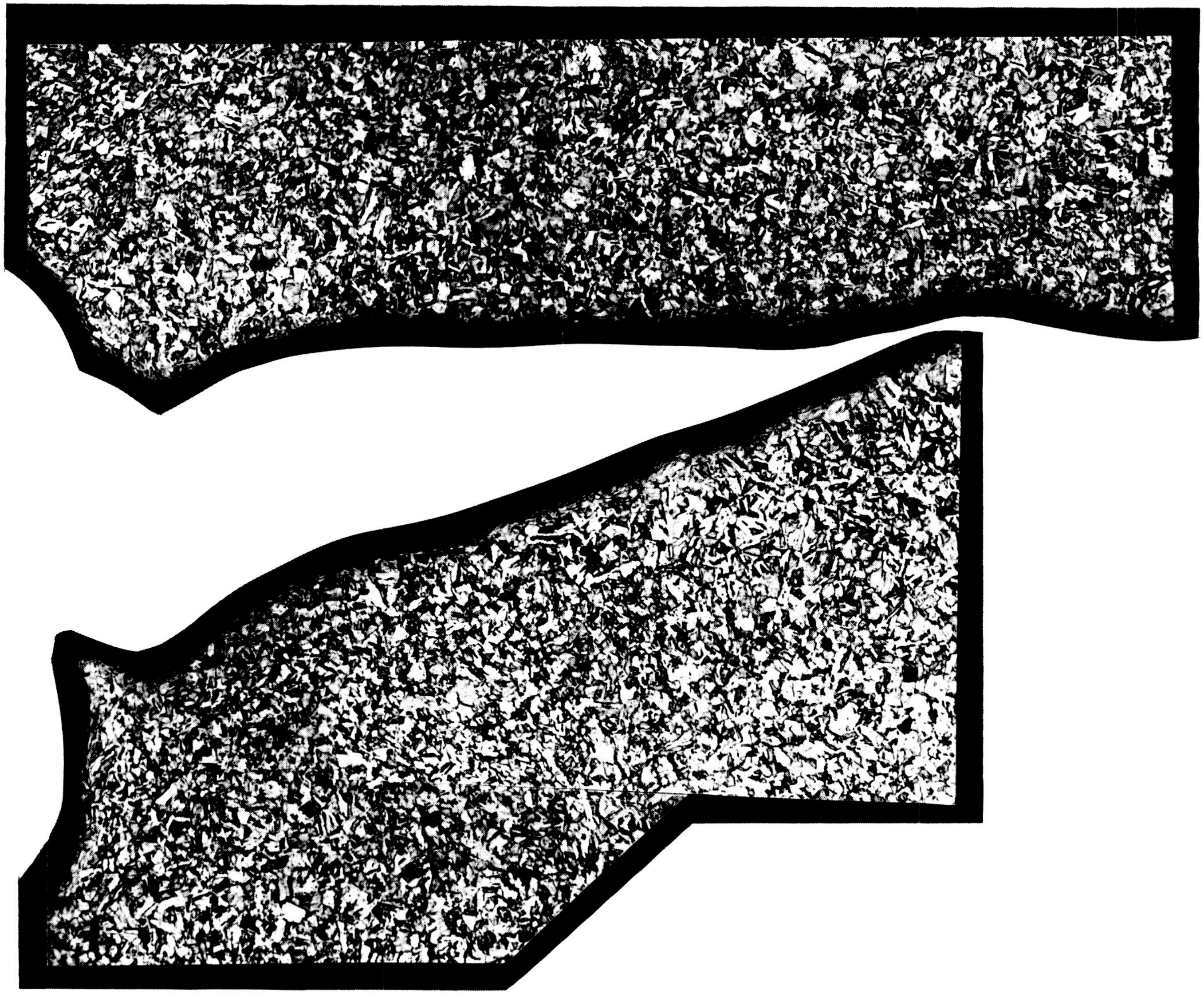

Figure 29. Section Through Fracture of Aged 18% Nickel Maraging Steel. Transverse Specimen SDT-10. Magnified 200 X, Etch Fry's Reagent (Mod.)

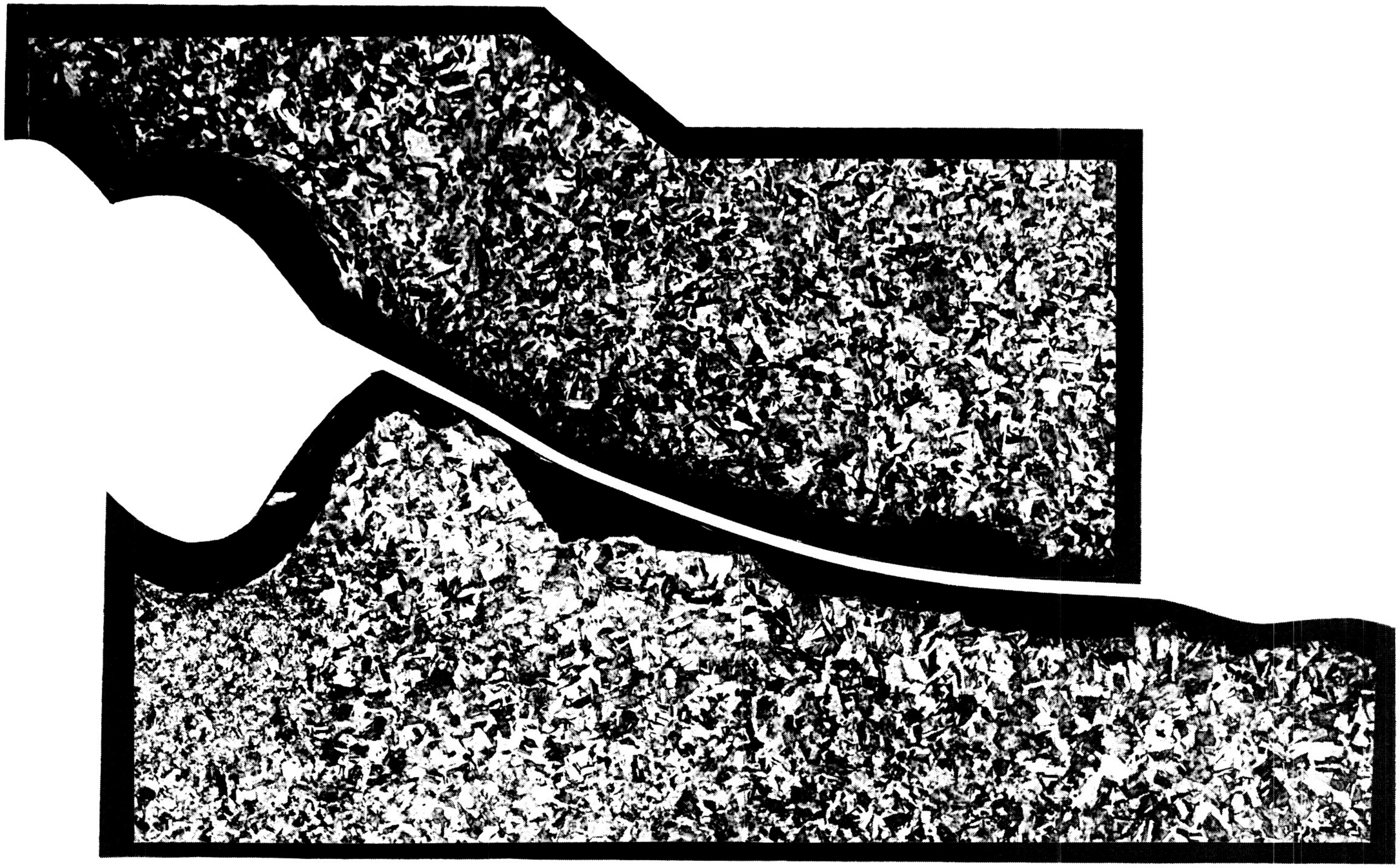

Figure 30. Section Through Fracture of Aged 18% Nickel Maraging Steel, Transverse Specimen SDT-12. Magnified 200 X, Etch Fry's Reagent (Mod.)

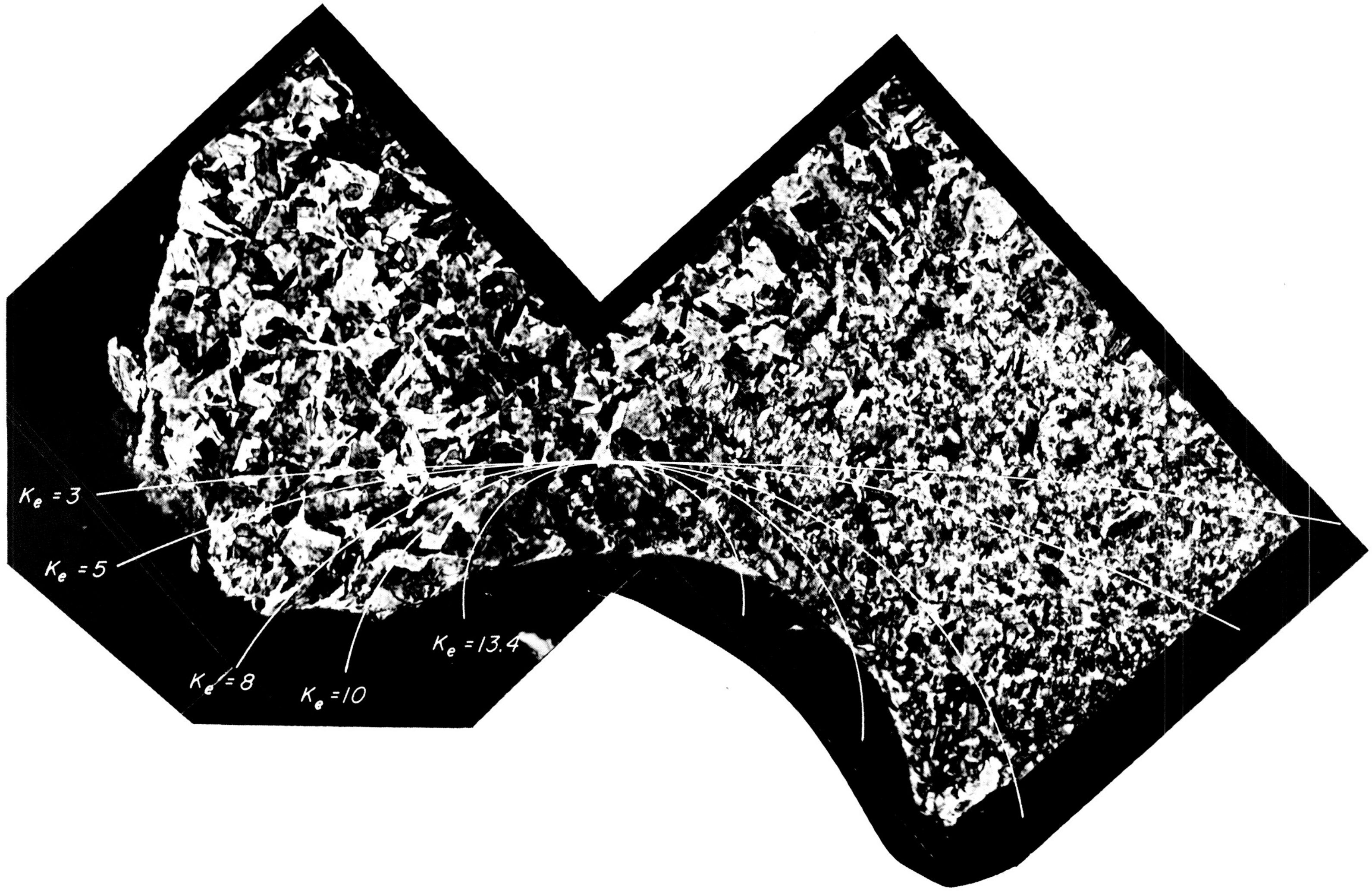

Figure 31. Enlargement of a Portion of Figure 30, Magnified 500 X with Superimposed Arc Segments Representing Hole Contours Which Would Produce the Values of k_e Shown.

6. Structural Design Considerations

Efficient design requires the use of the lightest weight structure to sustain the applied loads. The method of using the ductility ratio concept for making a rational choice of materials for efficient tension structure has been discussed previously in References (2) and (6). It involves determining structural strength/weight as a function of elastic stress concentration factor.

A comparison of the efficiencies of the two materials tested in the program can be made from Fig. 32, which has structural strength/weight on the ordinate and elastic stress concentration factor on the abscissa. The curves represent the upper limit of strength for structures containing the given elastic stress concentrations. Structures with a given k_e value must be designed to operate at a stress value lower than that represented by the curve.

In deriving the curves, the relation for plastic stress concentration factors, Eq. (11) was substituted into Eqs. (4) and (5). Assuming that notched strength corresponds to structural strength, S, and introducing the density, ρ

$$\frac{S}{\rho} = \frac{\sigma_{tu}}{\rho} \quad \text{for } k_e \leq k_{eo} \tag{12}$$

and

$$\frac{S}{\rho} = \frac{(\sigma_{tu}/\rho)}{1 + (k_e - k_{eo})\bar{e}} \quad \text{for } k_e > k_{eo} \tag{13}$$

The appropriate values of the constants obtained from the experiments were substituted into Eqs. (12) and (13) for each orientation in each material to obtain the data for the curves in Fig. 32. There were no test data for elastic concentration factor values for $k_e < 3$. Dashed lines are used from $k_e = 1$ representing the ultimate tensile strength to $k_e = 3$ to indicate the uncertainty of the interpolation in this region.

The assumption that the structural strength, S, is equivalent to the notched strength implies that the behavior of a notched tensile strip containing a given elastic stress concentration is representative of all tension structures of the same material and the same thickness having the same value of elastic stress concentration. Also implicit in the assumption is that a particular discontinuity characterized by an elastic stress concentration is equivalent in terms of its plastic and fracture behavior to all other discontinuities having the same value of elastic concentration factor regardless of the geometric configuration. Because of the influence of size-effects,

6320

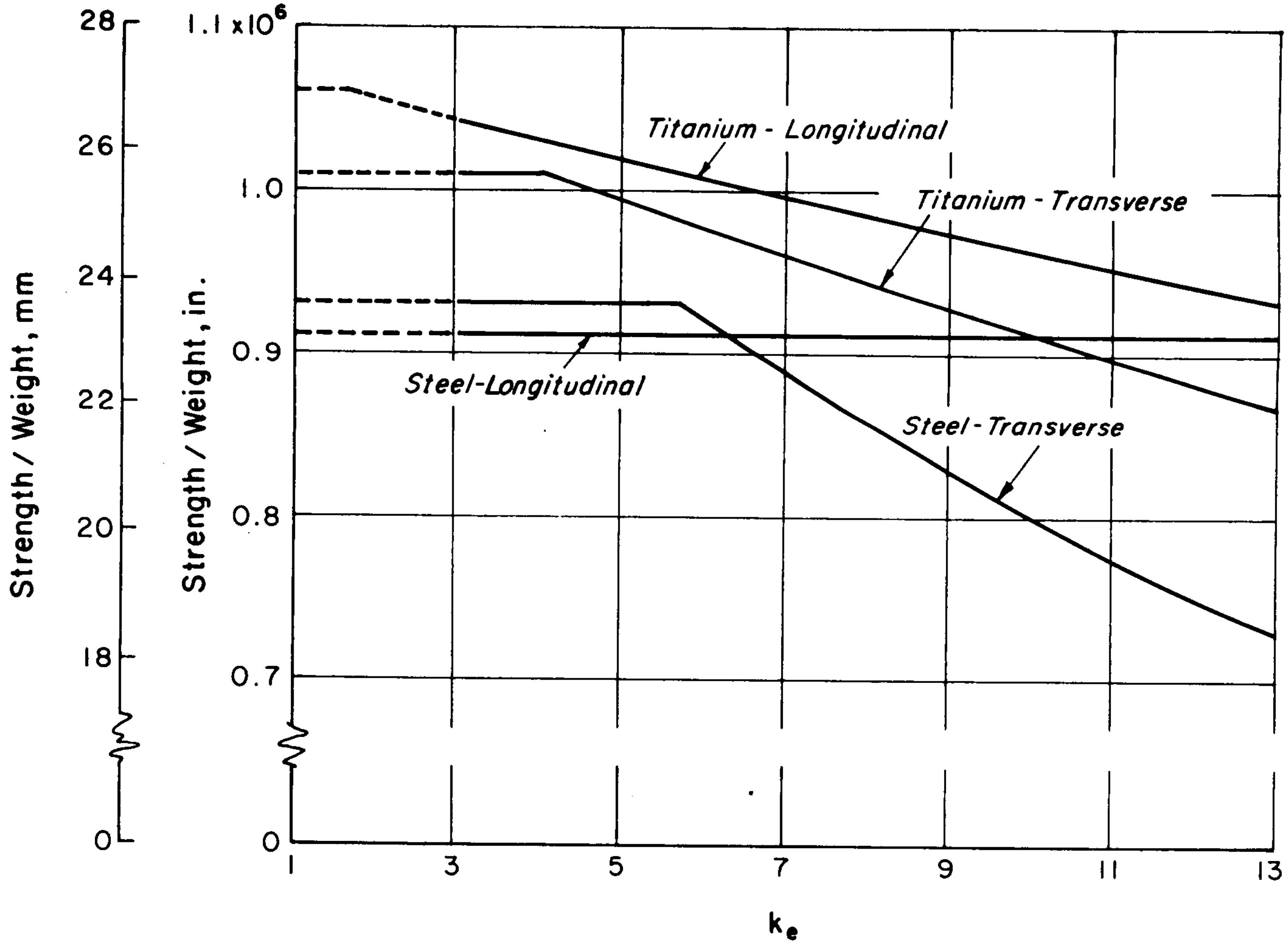

Figure 32. Strength/Weight of Tension Structures Containing Elastic Stress Concentrations of Aged Titanium Alloy Ti-6Al-4V, 0.045 in. (1.1 mm) thick and Aged 18% Nickel Maraging Steel, 0.040 in. (1.0 mm) thick.

the data for Fig. 32 would be pertinent to the thickness tested in this program. For other thicknesses additional tests would be necessary to obtain the necessary k_{eo} and $\bar{e}$ values.

It is clear from the data shown in Fig. 32 that anisotropy is an important consideration in efficient structural design. The longitudinally oriented titanium alloy Ti-6Al-4V material is more efficient than the transversely oriented titanium material. In the maraging steel the transversely oriented material is slightly more efficient than the longitudinally oriented material for k_e values up to 6.3 approximately. For higher values of k_e the longitudinal material is more efficient. Overall, the longitudinally oriented titanium is the most effieicent over the whole range of elastic stress concentration values tested.

Gerard (6) had originally hypothesized that the ultimate tensile strength/weight ratio could be related to the ductility ratio in limited ductility materials by an expression of the form

$$\sigma_{tu}/\rho = A\,\bar{e}^{1/6} \tag{14}$$

Since σ_{tu}/ρ has the dimension length and since $\bar{e}$ is dimensionless, the constant A will have the dimension length. For ordinary English engineering units σ_{tu}/ρ is expressed in inches and $A = 1.6 \times 10^6$ in. In the metric system, expressing σ_{tu}/ρ in millimeters, $A = 4.1 \times 10^7$ mm.

Values of the quantities in Eq. (14) were computed for the titanium alloy Ti-6Al-4V in both orientations and for the 18% nickel maraging steel in the transverse direction. The results are given in English units only in Table 10.

Table 10. Correlation of σ_{tu}/ρ and $1.6 \times 10^6 \bar{e}^{1/6}$ for Aged Titanium Alloy Ti-6V-4Al, L and T and Aged 18% Nickel Maraging Steel (250)

Material	Orientation	σ_{tu}/ρ - in.	$\bar{e}$	$1.6 \times 10^6 \bar{e}^{1/6}$ in.	Deviation Percent
Ti-6Al-4V	L	1.06×10^6	0.012	0.765×10^6	-31
Ti-6Al-4V	T	1.01×10^6	0.018	0.820×10^6	-18
Maraging Steel	T	0.93×10^6	0.038	0.930×10^6	0

Referring to Fig. 33, there are cryogenic data which also lie outside the $\pm$ 10% limits of Eq. (14). These deviations have not been explained, however, it should be noted that values of ductility ratio for these materials were obtained from the results of as few as three or four notch strength tests. This is in contrast to the 33-36 tests made for each of the analyses used in the current program.

Acknowledgements

The authors wish to acknowledge the contributions of the following Allied Research Associates staff members who participated in the programs: Mr. Richard Goldman for assistance in conducting the testing program and in analyzing the data; Mr. Joseph Furtado for machining the notch configurations in the specimens; Mr. Richard Lederman for the metallographic and photogrid preparations; Mr. Charles Lawnicki and Mr. Forrest Hewitt for manufacturing the specimen blanks.

We wish to thank Mr. Ward Minkler of TMCA who expedited our procurement of the titanium specimen material in the thickness we required for the program.

5907

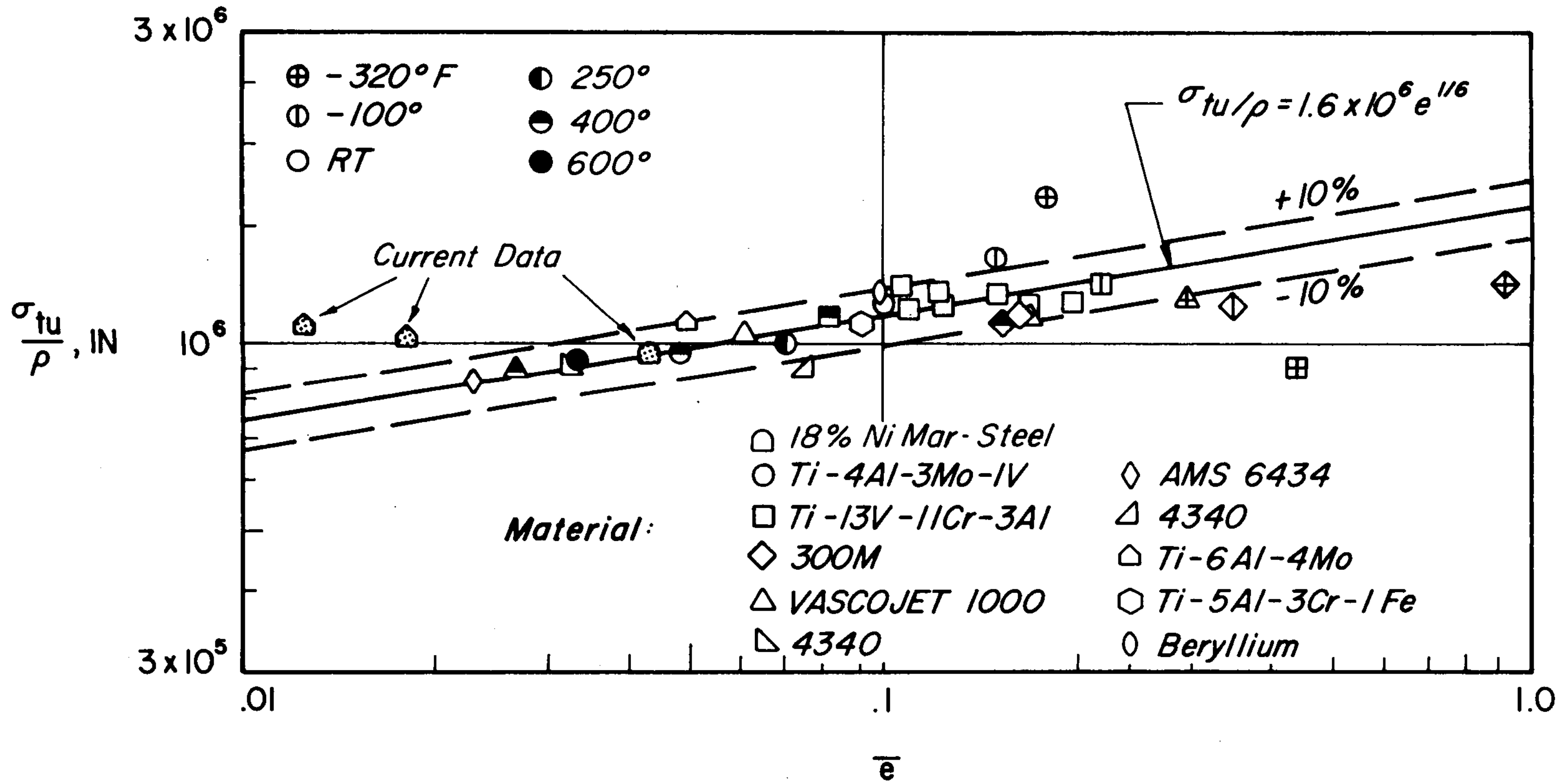

Figure 33. Material Strength/Weight Ratio as a Function of Ductility Ratio. Sources of the Notch Strength Data From which the Ductility Ratio Values were Derived as Follows: Ti-13V-11Cr-3Al Refs. 2, 3, 8; Ti-4Al-3Mo-1V, 300 M, Vascoject 1000 Ref. 7; Ti-5Al-3Cr-1V Ref. 8; Ti-6Al-4V Ref. 8 and current study; AMS 6434 Ref. 8; 4340 Refs. 8 and 9; Beryllium, Ref. 10.

REFERENCES

1. H. Hardrath and L. Ohman, "A Study of Elastic and Plastic Stress Concentration Factors Due to Notches and Fillets in Flat Plates," NACA Report No. 1117, 1953.

2. G. Gerard and R. Papirno, "Ductility Ratio of Aged All Beta Titanium Alloy," ASM Transactions Quarterly, Vol. 55, No. 3, pp. 373-388, September 1962.

3. R. Papirno, "Structural Ductility of High Strength Titanium Alloys." Presented at the ASTM Symposium on Applications Related Phenomena in Titanium Alloys, Los Angeles, Calif., April 18-19, 1967.

4. J. R. Dixon, "Stress Distribution Around a Central Crack in a Plate Loaded in Tension; Effect of Finite Width of Plate, "Journal of the Royal Aero. Society, Vol. 64, pp. 141-145, March 1960.

5. R. Papirno, "Stress Concentrations in Tensile Strips with Central Notches of Varying End Radii, "Journal of the Royal Aeronautical Society, Vol. 66, pp. 323-326, May 1962.

6. G. Gerard, "Structural Significance of Ductility in Aerospace Pressure Vessels," ARS Journal, Vol. 32, No. 8, pp. 1216-1221, August 1962.

7. V. Weiss, and J. Sessler, "Analysis of the Effects of Test Temperature on the Notch Strength of High Strength Sheet Alloys, "ASTM Preprint 80d, 1961.

8. G. Sachs, and J. Sessler, "Effect of Stress Concentration on Tensile Strength of Titanium and Steel Alloy Sheet at Various Temperatures," ASTM STP 287, pp. 122-137, (American Society for Testing Materials, Philadelphia, 1960).

9. V. Weiss, et al, "The Effect of Several Geometric Variables on the Notch Tensile Strength of 4340 Steel Sheet Heat Treated to Three Strength Levels, "WADD TR60-31, September 1960.

10. R. Crawford, F. and B. A. Burns, Bruce A., "Strength and Design Data for Beryllium Structures, "ASD TR 61-692, February 1962.

APPENDIX

APPENDIX

Table A1. Dimensions of Notched Specimens of Aged Titanium Alloy Ti-6Al-4V in the Longitudinal Direction

Specimen No.	Width in	Width mm	Ligaments a_1 in	Ligaments a_1 mm	Ligaments a_2 in	Ligaments a_2 mm	Thickness, t in	Thickness, t mm	Hole Diam. -2r in	Hole Diam. -2r mm
TFL-21	0.999	25.37	0.2983	7.57	0.2946	7.48	0.0437	1.11	0.125	3.18
TFL-9	0.999	25.37	0.2990	7.59	0.2899	7.36	0.0433	1.10	0.125	3.18
TFL-19	0.998	25.35	0.2932	7.44	0.2957	7.51	0.0438	1.11	0.125	3.18
TEL-4	0.998	25.35	0.3036	7.71	0.2952	7.49	0.0441	1.12	0.062	1.57
TEL-15	1.001	25.43	0.2946	7.48	0.3002	7.62	0.0436	1.10	0.062	1.57
TFL-11	0.998	25.35	0.2942	7.47	0.2944	7.47	0.0430	1.09	0.062	1.57
TFL-17	0.998	25.35	0.3051	7.75	0.2989	7.59	0.0422	1.07	0.036	0.91
TEL-17	0.999	25.37	0.2980	7.56	0.3055	7.76	0.0440	1.11	0.036	0.91
TFL-10	0.999	25.37	0.2992	7.60	0.2983	7.57	0.0433	1.10	0.036	0.91
TEL-1	0.999	25.37	0.3022	7.67	0.3026	7.68	0.0444	1.12	0.036	0.91
TEL-9	0.998	25.35	0.3065	7.78	0.3028	7.69	0.0438	1.11	0.024	0.61
TEL-13	0.998	25.35	0.3046	7.73	0.3019	7.66	0.0438	1.11	0.024	0.61
TFL-20	0.999	25.37	0.3078	7.81	0.3024	7.68	0.0425	1.08	0.024	0.61
TFL-16	0.999	25.37	0.3011	7.64	0.3003	7.62	0.0425	1.08	0.017	0.43
TFL-18	1.002	25.45	0.3010	7.64	0.3022	7.67	0.0427	1.08	0.017	0.43
TFL-8	0.999	25.37	0.2990	7.59	0.3016	7.66	0.0433	1.10	0.017	0.43
TEL-20	0.995	25.27	0.2956	7.50	0.3031	7.69	0.0439	1.11	0.013	0.33
TEL-8	1.000	25.40	0.3010	7.64	0.3023	7.67	0.0438	1.11	0.013	0.33
TEL-19	0.998	25.35	0.3032	7.70	0.3028	7.69	0.0441	1.12	0.013	0.33
TEL-18	0.995	25.27	0.3000	7.62	0.2998	7.61	0.0441	1.12	0.0098	0.25
TEL-11	1.000	25.40	0.3036	7.71	0.2998	7.61	0.0436	1.10	0.0098	0.25
TFL-7	0.995	25.27	0.3000	7.62	0.3001	7.62	0.0431	1.09	0.0098	0.25
TEL-16	0.993	25.22	0.2983	7.57	0.2983	7.57	0.0442	1.12	0.0079	0.20
TEL-12	0.995	25.27	0.2990	7.59	0.2957	7.51	0.0439	1.11	0.0079	0.20
TEL-10	0.997	25.32	0.2987	7.58	0.3014	7.65	0.0439	1.11	0.0079	0.20
TFL-4	1.000	25.40	0.2943	7.47	0.2997	7.61	0.0425	1.08	0.0066	0.17
TFL-14	1.000	24.40	0.2950	7.49	0.3000	7.62	0.0421	1.06	0.0066	0.17
TEL-5	1.000	25.40	0.2960	7.51	0.3005	7.63	0.0429	1.09	0.0055	0.14
TFL-5	1.000	25.40	0.2980	7.56	0.3006	7.63	0.0425	1.08	0.0055	0.14
TFL-6	1.000	25.40	0.3001	7.62	0.2999	7.61	0.0426	1.08	0.0046	0.12
TEL-6	1.000	25.40	0.3050	7.74	0.2978	7.56	0.0427	1.08	0.0046	0.12
TFL-2	1.000	25.40	0.3000	7.62	0.2980	7.56	0.0429	1.09	0.0042	0.11
TEL-2	1.000	25.40	0.3005	7.63	0.3000	7.62	0.0432	1.09	0.0042	0.11

Table A2. Dimensions of Notched Specimens of Aged Titanium Alloy Ti-6Al-4V in the Transverse Direction

Specimen No.	Width in	Width mm	Ligaments a_1 in	Ligaments a_1 mm	Ligaments a_2 in	Ligaments a_2 mm	Thickness, t in	Thickness, t mm	Hole Diam. -2r in	Hole Diam. -2r mm
TET-1	0.999	25.37	0.3009	7.64	0.2931	7.44	0.0443	1.12	0.125	3.18
TFT-6	0.999	25.37	0.2937	7.46	0.2986	7.58	0.9432	1.10	0.125	3.18
TFT-21	1.000	25.40	0.2981	7.57	0.3025	7.68	0.0430	1.09	0.125	3.18
TFT-1	0.997	25.32	0.2940	7.41	0.2938	7.46	0.043	1.10	0.062	1.57
TFT-7	0.999	25.37	0.2964	7.53	0.2919	7.41	0.044	1.13	0.062	1.57
TFT-8	0.999	25.37	0.2935	7.46	0.2988	7.59	0.044	1.12	0.062	1.57
TET-3	0.998	25.35	0.2935	7.55	0.3016	7.66	0.0438	1.11	0.036	0.91
TFT-13	0.999	25.37	0.3041	7.72	0.3060	7.77	0.0434	1.10	0.036	0.91
TET-4	0.997	25.32	0.3021	7.67	0.3045	7.73	0.0445	1.13	0.024	0.61
TFT-5	0.997	25.32	0.3034	7.71	0.3071	7.80	0.0431	1.10	0.024	0.61
TET-2	0.999	25.37	0.3070	7.80	0.3014	7.65	0.0440	1.12	0.024	0.61
TFT-15	0.999	25.37	0.3044	7.73	0.2967	7.53	0.0429	1.09	0.017	0.43
TET-21	1.000	25.40	0.2993	7.60	0.3021	7.67	0.0439	1.12	0.017	0.43
TFT-14	0.998	25.35	0.2997	7.61	0.3002	7.62	0.0431	1.10	0.013	0.33
TFT-20	0.997	25.32	0.2992	7.60	0.3043	7.73	0.0434	1.10	0.013	0.33
TFT-3	1.000	25.40	0.3049	7.74	0.3002	7.62	0.0428	1.09	0.013	0.33
TFT-18	0.997	25.32	0.3021	7.67	0.2985	7.58	0.0428	1.09	0.0098	0.25
TFT-19	0.994	25.25	0.2980	7.57	0.3005	7.63	0.0434	1.10	0.0098	0.25
TET-10	0.997	25.32	0.3004	7.63	0.3014	7.66	0.0440	1.12	0.0098	0.25
TFT-4	0.992	25.20	0.2979	7.57	0.2959	7.52	0.0432	1.10	0.0079	0.20
TET-6	0.996	25.30	0.3000	7.62	0.2986	7.58	0.0436	1.11	0.0079	0.20
TET-12	1.000	25.40	0.3045	7.73	0.2915	7.40	0.0432	1.10	0.0066	0.17
TET-11	1.000	25.40	0.2945	7.48	0.2970	7.54	0.0434	1.10	0.0066	0.17
TET-14	1.000	25.40	0.3058	7.77	0.2993	7.60	0.0434	1.10	0.0055	0.14
TET-13	1.000	25.40	0.3000	7.62	0.3015	7.66	0.0433	1.10	0.0055	0.14
TFT-16	1.000	25.40	0.3000	7.62	0.3045	7.73	0.0426	1.08	0.0046	0.12
TET-15	1.000	25.40	0.3045	7.73	0.2990	7.59	0.0426	1.08	0.0046	0.12
TET-17	1.000	25.40	0.3035	7.71	0.2995	7.61	0.0433	1.10	0.0042	0.11
TET-18	1.000	25.40	0.3043	7.73	0.3032	7.70	0.0429	1.09	0.0042	0.11

Table A3. Dimensions of Notched Specimens of Aged 18% Nickel Maraging Steel in the Longitudinal Direction

Specimen No.	Width in	Width mm	Ligaments a_1 in	Ligaments a_1 mm	Ligaments a_2 in	Ligaments a_2 mm	Thickness, t in	Thickness, t mm	Hole Diam. -2r in	Hole Diam. -2r mm
SDL-1	1.000	25.40	0.2982	7.57	0.2982	7.57	0.0404	1.03	0.125	3.18
SCL-1	1.000	25.40	0.2985	7.58	0.2976	7.56	0.0401	1.02	0.125	3.18
SDL-2	1.000	25.40	0.2972	7.55	0.2965	7.53	0.0402	1.02	0.125	3.18
SCL-2	0.999	25.37	0.3007	7.66	0.2996	7.61	0.0399	1.01	0.062	1.57
SCL-3	0.999	25.37	0.3019	7.67	0.3017	7.66	0.0402	1.02	0.062	1.57
SDL-3	0.999	25.37	0.3009	7.64	0.2996	7.61	0.0403	1.02	0.062	1.57
SCL-4	1.000	25.40	0.2959	7.52	0.2979	7.57	0.0400	1.02	0.036	0.91
SDL-4	0.999	25.37	0.2953	7.50	0.2974	7.55	0.0401	1.02	0.036	0.91
SDL-5	1.000	25.40	0.2981	7.57	0.2957	7.51	0.0402	1.02	0.036	0.91
SCL-5	1.001	25.43	0.3014	7.66	0.3013	7.65	0.0397	1.01	0.024	0.61
SDL-6	0.999	25.37	0.2998	7.62	0.3015	7.66	0.0400	1.02	0.024	0.61
SCL-6	1.000	25.40	0.3015	7.66	0.3021	7.67	0.0400	1.02	0.024	0.61
SCL-8	1.000	25.40	0.2905	7.38	0.2901	7.33	0.0400	1.02	0.017	0.43
SCL-9	1.000	25.40	0.2883	7.32	0.2903	7.37	0.0397	1.01	0.017	0.43
SDL-10	1.000	25.40	0.2917	7.41	0.2915	7.40	0.0401	1.02	0.017	0.43
SCL-12	1.000	25.40	0.2937	7.46	0.2939	7.46	0.0403	1.02	0.013	0.33
SDL-9	1.000	25.40	0.2947	7.48	0.2919	7.41	0.0404	1.03	0.013	0.33
SDL-7	1.000	25.40	0.2939	7.46	0.2944	7.48	0.0403	1.02	0.013	0.33
SCL-14	1.000	25.40	0.2975	7.56	0.2973	7.55	0.0402	1.02	0.0098	0.25
SCL-7	1.000	25.40	0.2962	7.52	0.2961	7.52	0.0402	1.02	0.0098	0.25
SDL-8	1.000	25.40	0.2957	7.51	0.2964	7.53	0.0403	1.02	0.0098	0.25
SCL-10	1.000	25.40	0.2965	7.53	0.2964	7.53	0.0398	1.01	0.0098	0.25
SCL-11	1.000	25.40	0.2978	7.56	0.3011	7.65	0.0404	1.03	0.0079	0.20
SCL-13	1.000	25.40	0.2950	7.49	0.2961	7.52	0.0404	1.03	0.0079	0.20
SGL-11	1.000	25.40	0.2980	7.57	0.3000	7.62	0.0396	1.01	0.0066	0.17
SGL-12	1.000	25.40	0.2985	7.58	0.3000	7.62	0.0398	1.01	0.0066	0.17
SHL-12	1.000	25.40	0.2991	7.60	0.3003	7.63	0.0395	1.00	0.0055	0.14
SHL-11	1.000	25.40	0.3015	7.66	0.3021	7.67	0.0398	1.01	0.0055	0.14
SGL-10	1.000	25.40	0.3030	7.70	0.3000	7.62	0.0395	1.00	0.0046	0.12
SGL-9	1.000	25.40	0.3000	7.62	0.2999	7.62	0.0395	1.00	0.0046	0.12
SHL-9	1.000	25.40	0.2997	7.61	0.2980	7.57	0.0398	1.01	0.0042	0.11
SHL-10	1.000	25.40	0.3000	7.62	0.2997	7.61	0.0396	1.01	0.0042	0.11

Table A4. Dimensions of Notched Specimens of Aged 18% Nickel Maraging Steel in the Transverse Direction

Specimen No.	Width in	Width mm	Ligaments a_1 in	Ligaments a_1 mm	Ligaments a_2 in	Ligaments a_2 mm	Thickness, t in	Thickness, t mm	Hole Diam. -2r in	Hole Diam. -2r mm
SCT-1	0.998	25.35	0.2973	7.55	0.2978	7.56	0.0400	1.02	0.125	3.18
SDT-2	0.998	25.35	0.2969	7.54	0.2969	7.54	0.0400	1.02	0.125	3.18
SDT-1	1.000	25.40	0.2962	7.52	0.2961	7.52	0.0400	1.02	0.125	3.18
SDT-3	0.998	25.35	0.3002	7.62	0.3007	7.66	0.0400	1.02	0.062	1.57
SCT-2	0.999	25.37	0.2999	7.62	0.3016	7.66	0.0398	1.01	0.062	1.57
SCT-3	0.998	25.35	0.3003	7.63	0.2995	7.61	0.0400	1.02	0.062	1.57
SDT-4	0.999	25.37	0.2966	7.53	0.2996	7.61	0.0400	1.02	0.036	0.91
SDT-5	0.998	25.35	0.2959	7.52	0.2985	7.58	0.0400	1.02	0.036	0.91
SCT-4	0.999	25.37	0.2976	7.56	0.2965	7.53	0.0400	1.02	0.036	0.91
SCT-6	1.000	25.40	0.3013	7.65	0.3013	7.65	0.0400	1.02	0.024	0.61
SCT-5	0.999	25.37	0.3002	7.62	0.3019	7.67	0.0398	1.01	0.024	0.61
SDT-6	0.997	25.32	0.3008	7.64	0.3005	7.63	0.0400	1.02	0.024	0.61
SDT-8	1.000	25.40	0.2934	7.45	0.2888	7.34	0.0401	1.02	0.017	0.43
SDT-15	1.000	25.40	0.2889	7.34	0.2882	7.32	0.0401	1.02	0.017	0.43
SDT-9	1.000	25.40	0.2886	7.33	0.2902	7.37	0.0401	1.02	0.017	0.43
SDT-16	1.000	25.40	0.2934	7.45	0.2940	7.47	0.0401	1.02	0.013	0.33
SCT-7	1.000	25.40	0.2927	7.44	0.2939	7.46	0.0400	1.02	0.013	0.33
SDT-17	1.000	25.40	0.2939	7.46	0.2945	7.48	0.0400	1.02	0.013	0.33
SDT-11	1.000	25.40	0.2952	7.50	0.2958	7.51	0.0400	1.02	0.0098	0.25
SDT-7	1.000	25.40	0.2962	7.52	0.2949	7.49	0.0401	1.02	0.0098	0.25
SDT-13	1.000	25.40	0.2964	7.53	0.3005	7.63	0.0403	1.02	0.0079	0.20
SDT-14	1.000	25.40	0.2942	7.47	0.2936	7.46	0.0401	1.02	0.0079	0.20
SDT-10	1.000	25.40	0.2944	7.48	0.2945	7.48	0.0400	1.02	0.0079	0.20
SDT-12	1.000	25.40	0.2954	7.50	0.2970	7.54	0.0402	1.02	0.0079	0.20
SGT-14	1.000	25.40	0.3010	7.64	0.3008	7.64	0.0397	1.01	0.0066	0.17
SGT-13	1.000	25.40	0.3008	7.64	0.3010	7.64	0.0396	1.01	0.0066	0.17
SHT-16	1.000	25.40	0.2983	7.58	0.3010	7.64	0.0395	1.00	0.0055	0.14
SHT-15	1.000	25.40	0.3025	7.68	0.2996	7.61	0.0398	1.01	0.0055	0.14
SHT-14	1.000	25.40	0.3000	7.62	0.3030	7.70	0.0394	1.00	0.0046	0.12
SHT-13	1.000	25.40	0.3000	7.62	0.3000	7.62	0.0396	1.01	0.0046	0.12
SGT-15	1.000	25.40	0.2982	7.57	0.2980	7.57	0.0398	1.01	0.0042	0.11
SGT-16	1.000	25.40	0.2955	7.51	0.2958	7.51	0.0394	1.00	0.0042	0.11

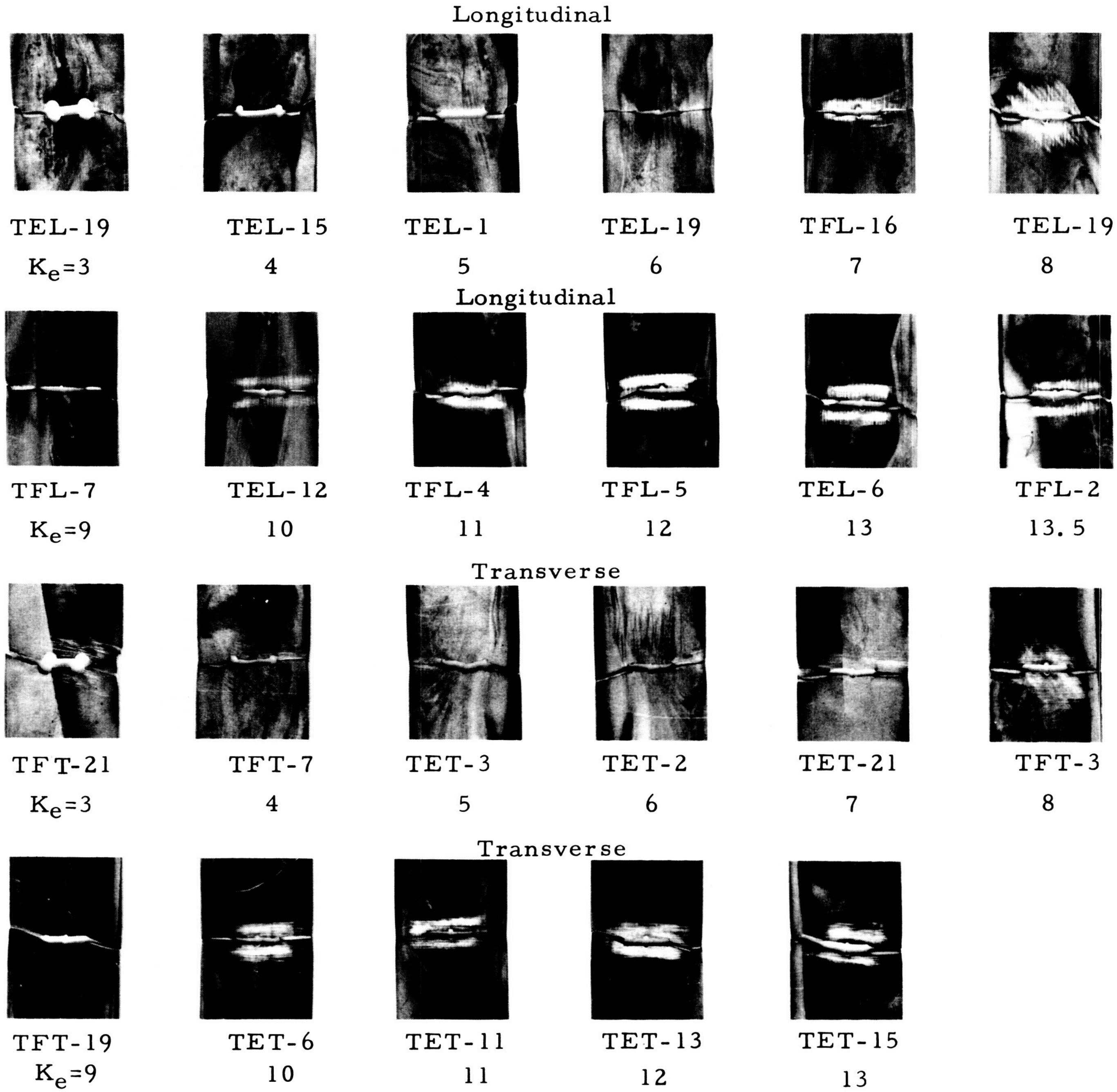

Figure A1 Tensile Fractures in Notched Specimens of Aged Titanium Alloy Ti-6 Al-4V Sheet - 0.045 inch (1.14mm) Thickness

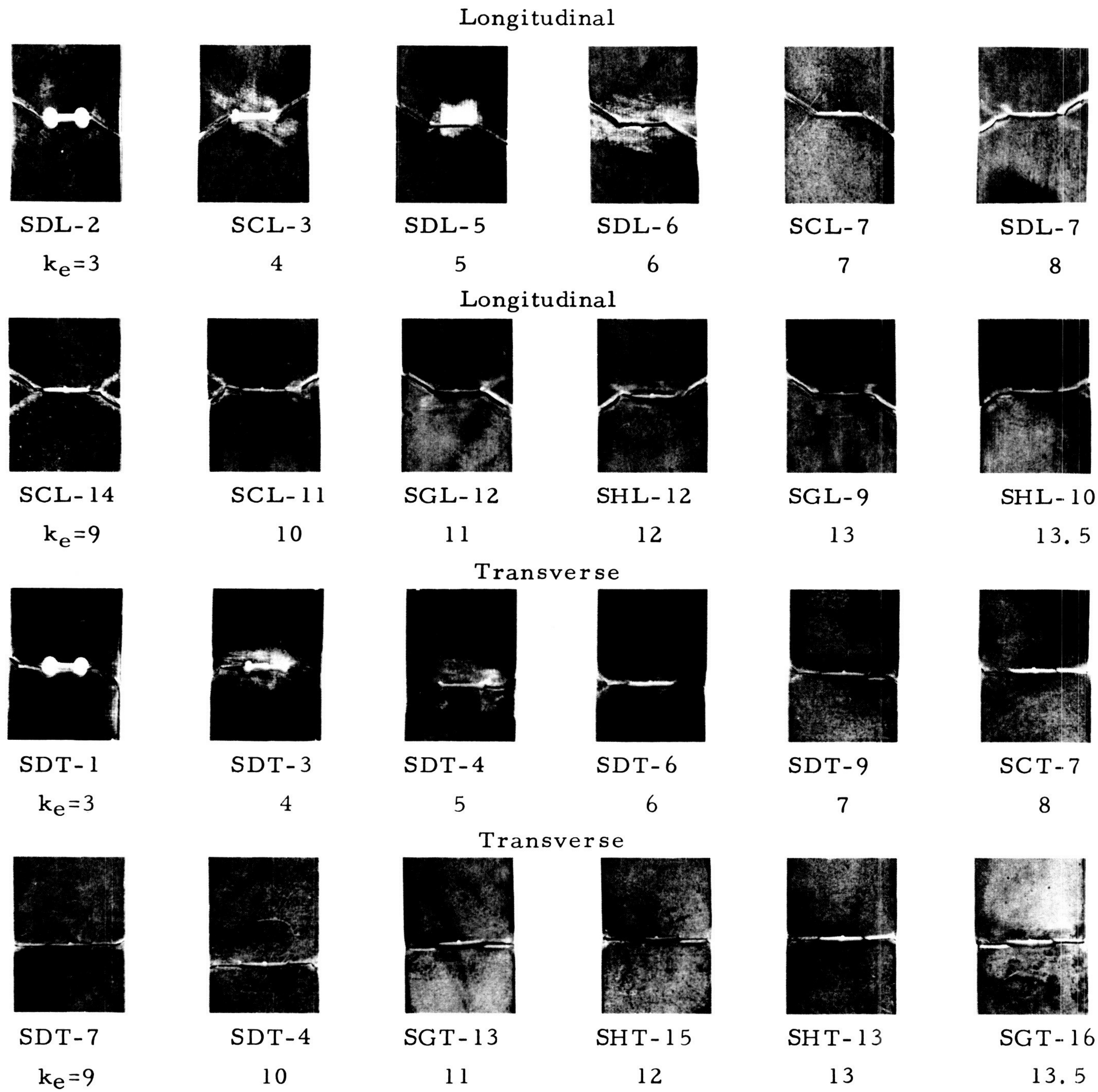

Figure A2 Tensile Fractures in Notched Specimens of Aged 18% Ni Maraging Steel (250) Sheet - 0.040 inch (1.01 mm) Thickness